NO. 31. INFRARED SPECTRA OF STARS AND PLANETS, IV: THE SPECTRUM OF MARS, 1-2.5 MICRONS, AND THE STRUCTURE OF ITS ATMOSPHERE*

by GERARD P. KUIPER

July 4, 1964

ABSTRACT

Spectra of the planet Mars obtained from the 82″ telescope of the McDonald Observatory are presented for the interval 1-2.5μ together with lunar comparisons and a limited set of laboratory calibrations. A full discussion of the CO_2 content of the Martian atmosphere and the surface pressure is given in the following two *Communications*. In this paper the IR spectra are examined for the presence of constituents other than CO_2 (CO, CH_4, NH_3, H_2S, NO, N_2O, HCHO, and COS), and for the presence of isotopic bands of CO_2. The O^{18} isotopic band at λ 2.15μ is definitely present in the Martian spectra and allows a provisional determination of the O^{18}/O^{16} ratio relative to the Earth. The evidence is strong, though not yet conclusive, that this ratio is larger on Mars than on the Earth. The other gases listed are all below the threshold of detection, with the upper limits found given in the text. The Martian spectral intensities are also expressed in terms of those derived for the Moon; the ratio spectra so obtained for Mars are summarized in Figure 25. In the introductory parts of the paper a discussion is given of the types of atmospheric particles detected in the Martian atmosphere and the information that may be derived therefrom. A rough value of the atmospheric pressure 10-20 mb is thus derived.

1. The Martian Atmosphere

The *presence* of a Martian atmosphere is shown by several well-known phenomena among which are: The variable and often local obscuration of surface detail; the variable appearance of the limb, including the occasional presence of clouds; the presence and seasonal variations of the polar caps and associated cloud phenomena; the occasional occurrence of white clouds and of yellow dust storms on the disk; the general veil observed in blue and ultraviolet light; and irregular polarization changes, correlated with the presence of varying haze. Two gases, CO_2 and H_2O, have been detected spectroscopically.

The *density* of this atmosphere has been uncertain. It has been widely held that a fair estimate was at hand from the interpretation of visual polarization measurements, notably by A. Dollfus. On the basis of all published data, de Vaucouleurs (1954, p. 125) concluded that the atmospheric surface pressure is 64 $\pm$ 3 mm or 85 $\pm$ 4 millibars (corresponding to an atmospheric mass of 0.20 terrestrial atmospheres or 1.6×10^5 cm NPT). Dollfus (1961, p. 387) similarly concluded that the pressure is near 90 millibars. This result, by the nature of its derivation, must actually be an *upper limit*. The violet layer that at all times surrounds the planet has been interpreted as due to particles because of its variable opacity

* Paper presented in outline at NASA Conference, Washington, D.C., October 1-2, 1963. The IR spectra were reviewed at the Liège Conference on Astrophysics, June 24-26, 1963 (Kuiper 1963).

near $\lambda = 0.45\ \mu$ (e.g., de Vaucouleurs, 1954, p. 55); and these particles must scatter in visual light also in a manner that would make it difficult to distinguish them from molecules.

We shall first examine what may be derived regarding the density of the Martian atmosphere from the presence of atmospheric particles and thereafter, from infrared spectroscopy.

2. *Atmospheric Particles: the Blue-Violet Haze*

The geometric albedo of Mars (measuring the brightness at opposition) is 0.154 in visual light ($\lambda = 0.554\ \mu$; Harris, 1961, p. 307) and 0.052 in the accessible ultraviolet (Harris, *loc. cit.;* effective wavelength: 0.353 μ). From the center-to-limb effect it may be estimated that the *atmospheric* contribution to the visual albedo does not exceed 0.02-0.03, whereas the absence of surface detail in the UV indicates that the atmospheric contribution to the UV albedo is 0.04 ± 0.01.

Dollfus's visual polarization data have been interpreted as due to an air mass of 0.2 terrestrial atmospheres in a vertical column, or 0.4 atm for the integrated disk. Since the back scattering of a tenuous gaseous atmosphere is $\frac{3}{8}\ \tau$, and at $\lambda = 0.55\ \mu$ the value of τ for the terrestrial atmosphere is 0.08 (Van de Hulst, 1952, p. 53), the computed atmospheric contribution to the visual albedo would be $\frac{3}{8} \times 0.08 \times 0.4 = 0.012$. The ratio of the assumed atmospheric scattering powers, UV to V, is then $(0.04 \pm 0.01)/0.012 = 3.3 \pm 1$, whereas molecular scattering would make the ratio $(.554/.353)^4 = 6.0$. However, the atmospheric component of the UV albedo cannot be all molecular in origin. The variable transparency of the Martian atmosphere near $\lambda = 0.45\ \mu$ and the spotty appearance of the best violet photographs (Humason, 1961, Plates 3-5) indicate that at the very most half the total UV albedo, or 0.026, can be of molecular origin, reducing the molecular contribution of the visual albedo to $0.026/6 = 0.004$. This reduces the *upper limit of the pressure* of the Martian atmosphere to about *30 millibars* at the very most. UV polarization data discussed below confirm this conclusion. Consistent with this interpretation of the UV albedo is the absence of a marked increase of reflectivity from 0.40 μ to 0.30 μ, noted on low-dispersion spectra taken with the 82-inch telescope. If molecular scattering alone were responsible, the intensity ratio 0.30 μ/0.40 μ relative to the Sun would be 3.2.

The other extreme assumption, that both the entire UV albedo and the visual atmospheric scattering are due to small particles, leads to an estimate of the particle size. If the particles are quartz ($n = 1.5$), a diagram by Van de Hulst (1952, p. 57) and the UV/V scattering ratio of 0.052/0.012 yield $(n\text{-}1)\pi d/\lambda \simeq 1$ for $\lambda = 0.35\ \mu$ and hence, $d = 0.22\ \mu$. If they are ice ($n = 1.31$) the dimension will be about 0.35 μ, in agreement with an earlier estimate made in this manner by Schatzman (1951) and a more complete discussion including Dollfus's visual polarization measures by Kuiper (1952, p. 393). Allowance for the Rayleigh scattering by the molecules and very small particles present, will make d slightly larger than the values stated. The estimate is rough because the differences between the phase functions at 0.35 and 0.55 μ have been neglected.

The Martian haze layer appears on the average to be higher over the tropics than over the polar zones. This follows from the abnormally-large ellipticity of the visual boundary of the planet (compared to the dynamical oblateness, which is well determined), a boundary that visual observation shows to be not the solid surface but *the top of the haze layer.* This observation is consistent with the observed atmospheric optical depth larger than unity for $\lambda \leq 4500$ Å, any possible wavelength dependence of opacity, and the large value of the air mass ($\simeq 40$) on the Martian limb at opposition. The excess height over the equator is about 17 km (Kuiper, 1952, p. 422), a value confirmed by additional measures of the visual oblateness made with the 82-inch telescope in 1956 and 1958. A roughly ellipsoidal haze distribution is to be expected from the thermally-driven convection in analogy with the latitude variation of the terrestrial tropopause level; and the associated vertical distributions of condensation products and dust. [My own observations would indicate that in summer the height of the terrestrial haze layer over continents is about 4-5 km at 30° N (region of McDonald Observatory), 3 km at 35° N (region of Albuquerque, N. M.), 2 km at 43° N (S. Wisconsin), and 0 km at the arctic circle. Above these levels the sky is of "coronographic" quality.]

If the Martian haze particles are ice, they are probably confined to the upper parts of the convective troposphere, where adiabatic cooling of surface air has led to supersaturation of water vapor. Denser clouds, if present, will occur in this same zone. If the particles were dust, they would extend downward with increasing concentration toward the surface. The presence of darker regions in the haze

layer having no correspondence to dark surface markings (Humason, *op. cit.*, Plates 3-5) may then be either thin darker dust clouds rising into the general haze layer or, more likely, veils of different-sized ice particles (see below).

It has sometimes been assumed that the greater strength of the blue veils and clouds toward the Martian limb is due to lower surface temperatures. This assumption is unwarranted. The average limb effect shown on UV photographs corresponds closely to the *secant of the air mass*. This is particularly well seen on Humason's 200-inch photographs which further show that the "lumpy" appearance of the veil is not limited to the limb but extends over the entire disk.

Systematic measurements of the reflectivity and polarization in the UV, coupled with high-resolution photography, can yield information on the *composition of the haze*. Only a few polarization measurements are yet available. They were made by Gehrels with the 82-inch telescope on 10 nights in 1959-61 (Gehrels and Teska, 1962, p. 173). Remarkable changes were detected, not correlated with phase, and therefore presumably due to variable particle size. For instance, at phase angle $\alpha = 43°3$ the polarization at 0.32 μ changed from 1.5% to 9.8% in 7 days (Aug. 22-29, 1960), while at 0.36 μ the polarization was found 0.1% at $\alpha = 43°3$ but 7.6% at $\alpha = 36°1$. *Rayleigh scattering by molecules*, which would cause a monotonic increase of polarization with α and show no time-variations, contributes therefore only *a minor fraction of the observed brightness*. The ever-changing veils and clouds must be largely responsible.

Gehrels' measures may be compared with theoretically-computed values for the above-mentioned alternative models of composition and particle diameter: quartz, $d \cong 0.22\ \mu$; and ice, $d \cong 0.35\ \mu$. I am much indebted to Dr. B. M. Herman of the Institute of Atmospheric Physics for making the computations. They are based on the Mie theory for spherical particles which Dr. Herman programmed for the IBM 7072. The computations yield the scattered intensities I_1 and I_2 in the two principal planes of polarization, from which the total intensities $I_1 + I_2$ and the polarizations, $P = (I_1 - I_2)/(I_1 + I_2)$ have been derived. Table 1 and Figure 1 show the first exploratory results, for quartz and ice (three diameters). The Gehrels measures quoted above were entered in Figure 1 to which was added a value for $\alpha = 35°$ taken from Figure 10 of the Gehrels-Teska paper, derived by a slight extrapolation of a well-defined relationship (to $\lambda^{-1} = 2.9$). It is seen that the Gehrels measures strongly favor *ice composition*, but that a much fuller investigation is warranted.

Figure 2 and Table 2 contain the data for spherical ice particles of 8 different dimensions, also based on Dr. Herman's computations. It is seen that for the smallest particles there is tendency toward alternation between the integral (2.0, 3.0) and half-integral (2.5, 3.5) values of the scattering parameter $2\pi a/\lambda$. If the different Martian veils shown on photographs each have very homogeneous composition in particle size, some very remarkable polarization contrasts may be expected in *high-resolution photography through a birefringent crystal*, provided that the wavelength band of the photography is kept narrow ($\triangle\lambda \simeq 300$ Å). This will be a very promising field of further study.

Presumably there will be some spread in the particle sizes in any one veil and certainly in low-resolution photography or photometry over the Martian disk. Therefore, it is of interest to determine the effect of *mixing* on the resultant polarization. Two types of mixtures are considered here, one of a fairly narrow spread in diameter and one a broader spread that automatically destroys the alternation effect cited above. The results are found in Table 3 and Figure 3. The mixtures are found by assigning the following weights to the 8 parameter values 2.0, 2.5, 3.0 . . . 5.5:

A: 1, 4, 10, 4, 1, 0, 0, 0; *B*: 0, 0, 1, 4, 10, 4, 1, 0; *C*: 0, 0, 0, 0, 1, 4, 10, 4 (these emphasize the *integral* values of $2\pi a/\lambda$).

A': 4, 10, 4, 1, 0, 0, 0, 0; *B'*: 0, 1, 4, 10, 4, 1, 0, 0; *C'*: 0, 0, 0, 1, 4, 10, 4, 1 (these emphasize the *half-integral* values).

A'': 2, 7, 10, 7, 2, 0, 0, 0; *B''*: 0, 0, 2, 7, 10, 7, 2, 0; *C''*: 0, 0, 0, 0, 2, 7, 10, 7 (these *balance* the integral and half-integral values).

At $\lambda = 0.35\ \mu$ the most frequent diameter is $d = 0.33\ \mu$ for mixtures *A* and *A''*, 0.44 μ for *B* and *B''*, and 0.56 μ for *C* and *C''*. A curve for $2\pi a/\lambda = 8$ is added to Fig. 3*a*. At $\lambda = 0.35\ \mu$ it corresponds to $d = 0.89\ \mu$. Such particles will appear *white* visually and occasional white clouds are seen on the planet.

The polarization curves in Figures 3*a* and 3*b* show that the effect of the alternation is still present, even for these mixtures. If the Martian veils (averaged over the finite areas observed) contain the assumed spread in particle sizes, then only $\alpha < 20°$ will yield interpretable results. For a larger spread, such as is assumed in Figure 3*c*, both $\alpha < 20°$ and $\alpha > 30°$ can be used. For a very small spread the

TABLE 1

Phase Angle	Polarization (%)					Total Intensity				
	A	B	C	D	E	A	B	C	D	E
0°.....	0.0	0.0	0.0	0.0	0.0	0.13722	0.44710	5.0827	0.51121	0.43792
5.....	0.0	— 0.9	— 2.6	— 0.4	— 0.4	0.13522	0.43305	4.8654	0.50547	0.43286
10.....	0.0	— 3.9	—10.6	— 1.6	— 1.6	0.12935	0.39349	4.2863	0.48866	0.41806
15.....	— 0.2	....	—23.8	....	....	0.11995	.....	3.5316	.....	.....
20.....	— 0.7	—16.1	—39.7	— 7.4	— 7.5	0.10762	0.27131	2.8193	0.42723	0.36415
25.....	— 1.9	—23.1	—50.7	—13.0	—13.2	0.09316	0.21303	2.3077	0.38703	0.32907
30.....	— 4.2	—22.5	—47.2	—21.1	—21.7	0.07756	0.17426	2.0377	0.34442	0.29212
35.....	— 8.6	— 4.1	—29.0	—32.7	—33.8	0.06195	0.16627	1.9352	0.30285	0.25643
40.....	—16.0	+27.1	— 4.8	—48.1	—50.0	0.04760	0.19662	1.8703	0.26609	0.22539
45.....	—26.9	+53.8	+19.4	—66.4	—69.0	0.03593	0.26781	1.7413	0.23811	0.20256
50.....	—37.4	+69.9	+42.2	—83.8	—86.5	0.02845	0.37668	1.5380	0.22302	0.19161
55.....	—34.2	+78.4	+62.6	—94.0	—95.6	0.02682	0.51435	1.3494	0.22509	0.19638
60.....	—11.1	+82.6	+72.9	—91.7	—91.6	0.03291	0.66686	1.3071	0.24881	0.22088
180.....	0.0	0.0	0.0	0.0	0.0	8.9902	95.723	830.36	17.589	16.765
					σ_S	.....	1.7109	.....	1.7510	1.6470
					σ_B	.....	9.0694	.....	2.6212	2.2454
					σ_B/σ_S	.....	5.3011	.....	1.4969	1.3633

Polarizations and total intensities ($I_1 + I_2$) for five types of spherical particles all computed for $\lambda = 0.35\mu$: (A) ice ($n = 1.31$), $2\pi a/\lambda = 2.09$, $d = 2a = 0.233\ \mu$; (B) ice, $d = 0.35\ \mu$; (C) ice, $d = 0.525\ \mu$ (D) quartz ($n = 1.50$), $d = 0.22\ \mu$, no absorption; (E) as (D), $K = 0.01$ (weak absorption).

TABLE 2a

Phase Angle	2.0	2.5	3.0	3.5	4.0	4.5	5.0	5.5
0°.....	0.0	0.0	0.0	0.0	0.0	0.0	0.0	0.0
5	+ 0.0	+ 0.2	— 0.1	— 0.8	— 0.7	— 3.2	— 2.4	— 8.9
10	+ 0.1	+ 0.9	— 0.0	— 3.2	— 2.4	—13.2	— 8.7	—36.7
15	+ 0.1	+ 1.9	+ 0.7	— 7.5	— 3.8	—31.2	—14.4	—67.4
20	0.0	+ 3.3	+ 3.4	—14.3	— 2.1	—55.1	—11.9	—40.6
25	— 0.2	+ 5.0	+10.0	—24.4	+ 5.5	—71.2	+ 1.8	+21.2
30	— 0.3	+ 6.7	+22.0	—38.2	+18.7	—54.4	+19.1	+61.0
35	+ 0.6	+ 8.1	+38.2	—54.5	+33.1	— 9.8	+31.9	+81.6
40	+ 5.2	+ 8.8	+54.4	—68.3	+44.4	+33.0	+37.5	+91.0
45	+18.7	+ 8.0	+66.7	—70.0	+50.7	+63.0	+34.4	+89.0
50	+41.1	+ 4.6	+74.3	—52.5	+52.0	+81.7	+17.9	+67.6
55	+61.1	— 2.8	+77.8	—21.0	+47.9	+90.5	—20.0	+18.6
60	+71.9	—15.7	+78.4	+13.2	+36.4	+87.7	—47.6	—35.2
65	+76.4	—34.4	+76.7	+41.8	+13.3	+70.1	— 2.5	—54.8
70	+77.7	—55.9	+72.7	+62.1	—25.2	+36.6	+37.7	—40.8
75	+77.4	—71.5	+66.2	+73.7	—58.6	— 7.0	+53.1	—10.4
80	+75.9	—70.7	+56.0	+76.9	—40.1	—46.2	+54.3	+21.3
85	+73.5	—51.7	+40.6	+72.7	+ 0.9	—61.7	+43.4	+37.3
90	+70.1	—24.7	+16.9	+61.6	+26.6	—44.5	+14.4	+31.0
95	+65.8	— 0.5	—16.7	+43.5	+37.7	—11.0	—42.5	+ 9.2
100	+60.9	+16.5	—48.7	+17.0	+39.9	+15.1	—76.2	—21.2
105	+55.4	+26.2	—50.6	—18.5	+36.0	+26.6	—34.1	—46.7
110	+49.5	+30.4	—27.4	—52.6	+25.7	+26.8	+ 1.5	—38.3
115	+43.6	+31.0	— 6.3	—56.5	+ 5.3	+18.9	+16.0	—10.3
120	+37.6	+29.3	+ 5.4	—32.0	—29.1	+ 3.1	+18.5	+ 5.7
125	+31.9	+26.4	+10.6	— 9.8	—50.3	—22.6	+12.3	+ 9.3
130	+26.5	+22.8	+12.1	+ 1.8	—32.1	—42.4	— 6.4	+ 5.0
135	+21.5	+19.0	+11.6	+ 6.5	—12.8	—28.4	—38.4	— 8.4
140	+17.0	+15.3	+10.2	+ 7.6	— 3.2	—12.0	—37.1	—28.2
145	+13.0	+11.8	+ 8.3	+ 7.0	+ 0.7	— 1.8	—16.3	—23.0
150	+ 9.5	+ 8.7	+ 6.4	+ 5.8	+ 2.0	+ 1.1	— 5.8	— 9.2
155	+ 6.6	+ 6.1	+ 4.6	+ 4.3	+ 2.0	+ 1.8	— 1.7	— 3.0
160	+ 4.2	+ 4.0	+ 3.0	+ 2.9	+ 1.6	+ 1.5	— 0.2	— 0.8
165	+ 2.4	+ 2.2	+ 1.7	+ 1.6	+ 1.0	+ 1.0	+ 0.2	— 0.1
170	+ 1.1	+ 1.0	+ 0.8	+ 0.7	+ 0.5	+ 0.5	+ 0.2	+ 0.1
175	+ 0.3	+ 0.2	+ 0.2	+ 0.2	+ 0.1	+ 0.1	+ 0.5	+ 0.03
180	0.0	0.0	0.0	0.0	0.0	0.0	0.0	0.0

Polarization (%) of spherical ice particles for values of the scattering parameter $2\pi a/\lambda = 2.0$-5.5.

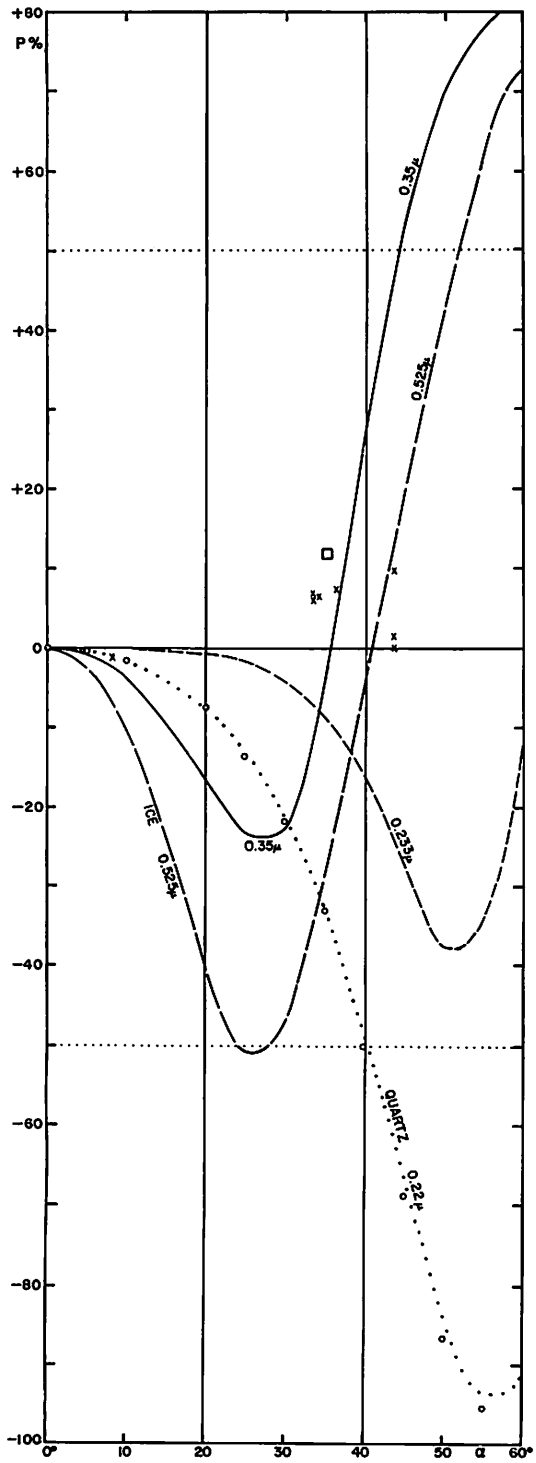

Fig. 1. Computed polarizations for sub-micron ice and quartz spheres if observed at $\lambda = 0.35\ \mu$ (cf. Table 1). Polarization measures of Mars from Gehrels and Teska, 1962.

results will be complex (Figures 2*a-d*).

The extremely-strong forward scattering of the haze particles will give Mars in the far UV some properties resembling Venus in visual light; i.e., the *phase integral in the UV will be larger than in the visual* and the Martian Bond albedo at 0.35 μ will be about 0.07, not 0.05. It is also seen from the backscattering coefficients of Table 2 that variations in particle size alone can produce large variations in surface brightness over the planetary disk.

A further estimate of the total molecular content of the Mars atmosphere can come from the albedo of the planet in the *far* UV, at wavelengths so short that the molecular scattering exceeds the particle scattering. Where this occurs may be estimated as follows: the extinction coefficient for pure air at 0° C and 1 atm pressure is 10^{-7} cm^{-1} at 5740 Å (Van de Hulst 1952, p. 55) or 10^{-9} cm^{-1} at 10 mb. If the Martian scale height is 20 km, the molecular extinction coefficient for the Martian atmosphere becomes 2.10^{-3} per 10 mb of surface pressure. The molecular contribution to the albedo for a uniform disk (2 air masses average) will be $2 \times 3/8$ of the extinction or about 0.0016 per 10 mb at $\lambda = 0.57\ \mu$ or, by the λ^{-4} law, 0.23 per 10 mb at $\lambda = 0.15\ \mu$. Well below 0.18 μ the ice particles will be nearly opaque. Table 3 shows Dr. Herman's computations of the scattering by both transparent and nearly-opaque particles for which $2\pi a/\lambda = 8$; at $\lambda = 0.15\ \mu$ the corresponding particle size is $d = 0.38\ \mu$; at $\lambda = 0.12\ \mu$ it is $d = 0.306\ \mu$. Therefore, the computations apply to ice particles of about 0.35 μ diameter, as found to be present, when observed in the 0.12-0.15 μ region. The computed backscattering per unit solid angle of these particles in terms of total scattering, is 0.044 for transparent particles and 0.186 for particles with the absorption coefficient $k = 1.0$; and 0.138 for $k = 0.765$. These values suggest that observations designed to determine the *total molecular scattering* in the Martian atmosphere may be optimum at the shortest wavelength at which the haze particles are still transparent, i.e., about 0.18 μ.

It is of interest to note that the *Martian blue haze may be simulated* in the laboratory. This may be done by pumping liquid nitrogen into an open vessel placed in very dry air, such as a mountain-observatory site has in winter. The evaporating nitrogen then freezes the atmospheric water vapor into sub-micron ice crystals producing a *blue* cloud, much like light smoke. If the atmospheric water-vapor content is larger, a white cloud is produced

TABLE 2b

Phase Angle	2.0	2.5	3.0	3.5	4.0	4.5	5.0	5.5
0°	0.062944	0.69815	0.35503	1.9472	1.6997	3.1703	4.2673	3.5196
5	0.061821	0.69271	0.34976	1.9023	1.6539	3.0109	4.0904	3.1781
10	0.058541	0.67662	0.32832	1.7739	1.5323	2.5850	3.6596	2.4107
15	0.053368	0.65063	0.30048	1.5796	1.3770	2.0297	3.2154	1.8090
20	0.046734	0.61587	0.27098	1.3453	1.2422	1.5151	2.9947	1.8867
25	0.039222	0.57389	0.24754	1.1005	1.1753	1.1822	3.0850	2.7193
30	0.031552	0.52644	0.23779	0.87387	1.1998	1.0952	3.3635	3.8852
35	0.024561	0.47547	0.24808	0.68856	1.3056	1.2267	3.5596	4.7451
40	0.019192	0.42297	0.28224	0.55966	1.4500	1.4800	3.4108	4.8588
45	0.016484	0.37093	0.34081	0.49341	1.5704	1.7358	2.8274	4.2515
50	0.017581	0.32125	0.42051	0.48826	1.6038	1.9013	1.9736	3.3533
55	0.023751	0.27582	0.51421	0.53740	1.5108	1.9412	1.2087	2.6743
60	0.036439	0.23660	0.61134	0.63169	1.2934	1.8771	0.91878	2.4674
65	0.057333	0.20593	0.69891	0.76183	1.0044	1.7620	1.3055	2.6266
70	0.088463	0.18690	0.76299	0.91876	0.74230	1.6479	2.2538	2.8765
75	0.13232	0.18409	0.79092	1.0920	0.63140	1.5691	3.3485	3.0689
80	0.19196	0.20438	0.77441	1.2661	0.78845	1.5562	4.0547	3.3087
85	0.27112	0.25807	0.71383	1.4181	1.2816	1.6699	4.0018	3.7811
90	0.37429	0.36005	0.62376	1.5177	2.0902	2.0271	3.2526	4.4416
95	0.50664	0.53092	0.53990	1.5365	3.0784	2.7780	2.4179	4.9356
100	0.67390	0.79773	0.52670	1.4679	4.0015	4.0125	2.5028	4.9882
105	0.99206	1.1941	0.68464	1.3626	4.5632	5.6210	4.4514	5.0673
110	1.1369	1.7589	1.1548	1.3735	4.5411	7.1987	8.5026	6.6489
115	1.4432	2.5345	2.1184	1.8050	3.9791	8.1312	13.665	11.412
120	1.8041	3.5603	3.7872	3.1467	3.4177	7.9841	17.776	19.452
125	2.2202	4.8708	6.3842	6.0736	4.0953	7.2059	18.583	27.842
130	2.6885	6.4847	10.112	11.390	8.0210	7.9582	15.922	31.693
135	3.2020	8.3992	15.108	19.908	17.813	14.671	14.359	29.035
140	3.7489	10.584	21.405	32.257	36.232	33.822	24.890	28.190
145	4.3129	12.975	28.884	48.671	65.439	72.569	63.957	52.923
150	4.8736	15.476	37.253	68.782	106.10	136.30	148.74	139.36
155	5.4076	17.962	46.041	91.502	156.66	225.75	289.39	321.69
160	5.8898	20.287	54.631	115.15	212.96	334.75	481.09	610.52
165	6.2958	22.300	62.327	137.09	268.61	449.89	699.88	975.20
170	6.6036	23.859	68.434	155.17	316.03	552.69	905.83	1342.4
175	6.7957	24.845	72.365	167.06	347.97	624.08	1053.6	1617.2
180	6.8611	25.182	73.721	171.20	359.25	649.66	1107.4	1719.3
σ_S	0.61996	1.0763	1.5528	2.0554	2.5616	2.9683	3.3787	3.6289
σ_B	0.03147	0.22341	0.07889	0.31792	0.21247	0.31312	0.34138	0.23270
σ_B/σ_S	0.051	0.207	0.051	0.155	0.083	0.106	0.101	0.064

Total scattering intensity of spherical ice particles for values $2\pi a/\lambda = 2.0$-5.5; σ_S = total scattering, σ_B = back scattering, both in terms of πa^2.

TABLE 3a

Phase Angle	Polarization (%)				Total Intensity					
	A	B	C	D	A	B	C	D	E	F
0°	0.0	0.0	0.0	0.0	0.37904	1.0523	1.8877	4.9230	8.8937	5.9679
5	− 0.4	− 1.0	− 3.7	−51.0	0.77878	2.0315	3.5428	3.9300	8.8155	5.9101
10	− 1.6	− 6.2	−14.0	−73.7	0.73381	1.8373	3.0585	5.0046	8.5959	5.7654
15	− 3.4	−12.9	−24.7	+ 6.2	0.67780	1.5861	2.5730	12.381	8.2920	5.5658
20	− 5.3	−15.5	−22.3	+42.2	0.59216	1.3565	2.3577	20.293	8.0258	5.4282
25	− 6.2	−13.3	+ 9.7	+59.3	0.51937	1.2108	2.5069	19.047	7.9589	5.4273
30	− 4.8	− 3.3	+25.1	+72.2	0.46053	1.1738	2.8819	9.6889	8.1707	5.5725
35	+ 0.4	+14.6	+44.1	+68.6	0.42233	1.2262	3.1994	4.1785	8.5191	5.7515
40	+ 9.7	+31.5	+54.3	+48.1	0.41111	1.3176	3.2059	9.0643	8.6833	5.7934
45	+21.5	+43.8	+55.8	+44.4	0.42262	1.3894	2.8312	16.383	8.4664	5.6408
50	+33.1	+50.7	+46.6	−30.8	0.45323	1.3995	2.2294	15.411	8.0864	5.4624
55	+42.9	+52.2	+22.8	+21.2	0.49647	1.3373	1.6874	7.8383	8.0372	5.5154
60	+50.2	+47.6	+ 2.8	−87.4	0.54582	1.2249	1.4663	4.2914	8.5087	5.8276
180	0.0	0.0	0.0	0.0	94.443	402.86	1045.48	6444.8	3371.6	3171.25
				σ_S	1.5618	2.4921	3.3020	3.5124	1.4899	1.3548
				σ_B	5.2910	2.8896	3.0577	1.5384	0.27793	0.18650
				σ_B/σ_S	3.3877	1.1595	0.92601	0.43799	0.18789	0.13766

Polarizations and intensities for three mixtures of spherical ice particles defined in the text and $2\pi a/\lambda = 8$ (D, no absorption; E, $K = 1.0$; F, $K = 0.765$).

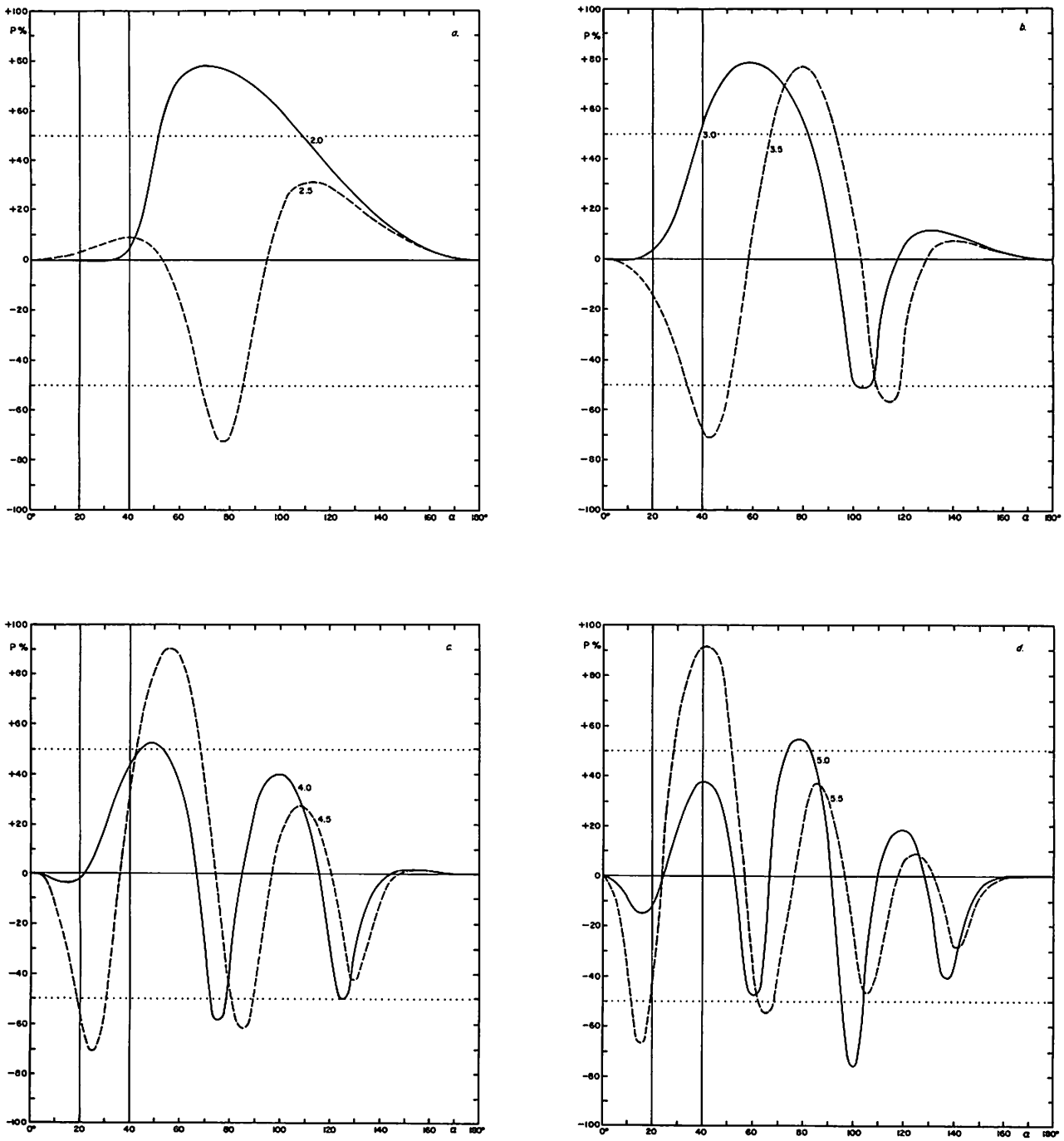

Fig. 2. Computed polarization curves for sub-micron ice spheres with eight values of the scattering parameter $2\pi a/\lambda$, entered in the figures (cf. Table 2).

TABLE 3b

POLARIZATION AND INTENSITIES FOR THREE MIXTURES OF SPHERICAL ICE PARTICLES DEFINED IN THE TEXT

PHASE ANGLE	POLARIZATION (%)			TOTAL INTENSITY		
	A′	B′	C′	A′	B′	C′
0°	0.0	0.0	0.0	0.55797	1.5869	3.0519
5	0.0	— 0.9	— 3.1	0.55098	1.5367	2.9083
10	0.0	— 3.7	—11.3	0.53093	1.4222	2.5401
15	— 0.1	— 8.9	—23.2	0.50007	1.2623	2.1028
20	+ 0.5	—13.0	—30.7	0.46183	1.0818	1.7665
25	+ 1.4	—17.0	—17.2	0.42034	0.92262	1.6342
30	+ 3.1	—17.3	— 1.3	0.37977	0.80553	1.6982
35	+ 6.0	—11.7	+23.1	0.34388	0.74012	1.8581
40	+10.2	— 0.8	+41.9	0.31553	0.72144	1.9831
45	+15.6	+12.0	+54.0	0.29641	0.73427	1.9847
50	+21.5	+23.6	+60.0	0.28701	0.76013	1.8582
55	+27.0	+32.6	+59.3	0.28671	0.78455	1.6751
60	+31.0	+38.9	+51.5	0.29415	0.80247	1.5359
180	0.0	0.0	0.0	39.145	205.94	7126.94
			σ_S	2.3067	2.0528	2.9565
			σ_B	3.6666	3.8607	2.4486
			σ_B/σ_S	1.5895	1.8807	0.82822

TABLE 3c

POLARIZATIONS AND INTENSITIES FOR THREE MIXTURES OF SPHERICAL ICE PARTICLES DEFINED IN THE TEXT

PHASE ANGLE	POLARIZATION (%)			TOTAL INTENSITY		
	A″	B″	C″	A″	B″	C″
0°	0.0	0.0	0.0	0.91405	2.2166	3.5731
5	— 0.5	— 1.8	— 4.3	0.89559	2.1360	3.2522
10	— 1.8	— 7.0	—15.8	0.84352	1.9218	2.8704
15	— 3.8	—14.5	—28.7	0.76704	1.6452	2.3761
20	— 6.1	—20.9	—26.4	0.67913	1.3920	2.1632
25	— 7.8	—20.6	+ 6.4	0.59375	1.2285	2.3273
30	— 7.6	— 8.7	+27.2	0.52296	1.1780	2.7268
35	— 4.1	+ 9.7	+47.6	0.47461	1.2171	3.0773
40	+ 3.2	+27.8	+59.5	0.45140	1.2916	3.1299
45	+13.2	+41.5	+62.0	0.45115	1.3444	2.8202
50	+23.8	+50.0	+53.5	0.46838	1.3412	2.2971
55	+33.4	+53.1	+31.2	0.49656	1.2823	1.8237
60	+44.1	+50.3	+ 4.8	0.53040	1.1984	1.6225
180	0.0	0.0	0.0	101.58	416.78	1091.38
			σ_S	1.9635	2.5230	3.2727
			σ_B	4.5475	3.1438	2.9460
			σ_B/σ_S	2.3161	1.2460	.90015

(larger crystals). Filter observations of objects seen through such a blue cloud duplicate very well the wavelength dependence of extinction by the Martian haze. Shadows cast by these blue clouds are brownish. An effort will be made in collaboration with Professor Alvar Wilska to make electron micrograms of these blue particles.

In summary, we find (1) the molecular content of the Mars atmosphere cannot be determined from visual polarization measurements; (2) *the surface atmospheric pressure is well below 30 millibars*. A sharper limit can be derived from further UV measures.

3. *Atmospheric Particles: General*

In addition to the blue-violet haze layer and the whitish clouds embedded in it, one occasionally observes *yellowish dust clouds*. Excellent photographs of such clouds are found in a chapter by Finsen (1961). These clouds set broad density limits on the Martian atmosphere because they are both generated and upheld by aerodynamic forces. The absence of rain on Mars will result in a much longer residence time of fine particulate matter in the atmosphere, and part of the UV haze layer could be remnants of dust storms. I am much indebted to Dr. James E. McDonald of the Institute of Atmos-

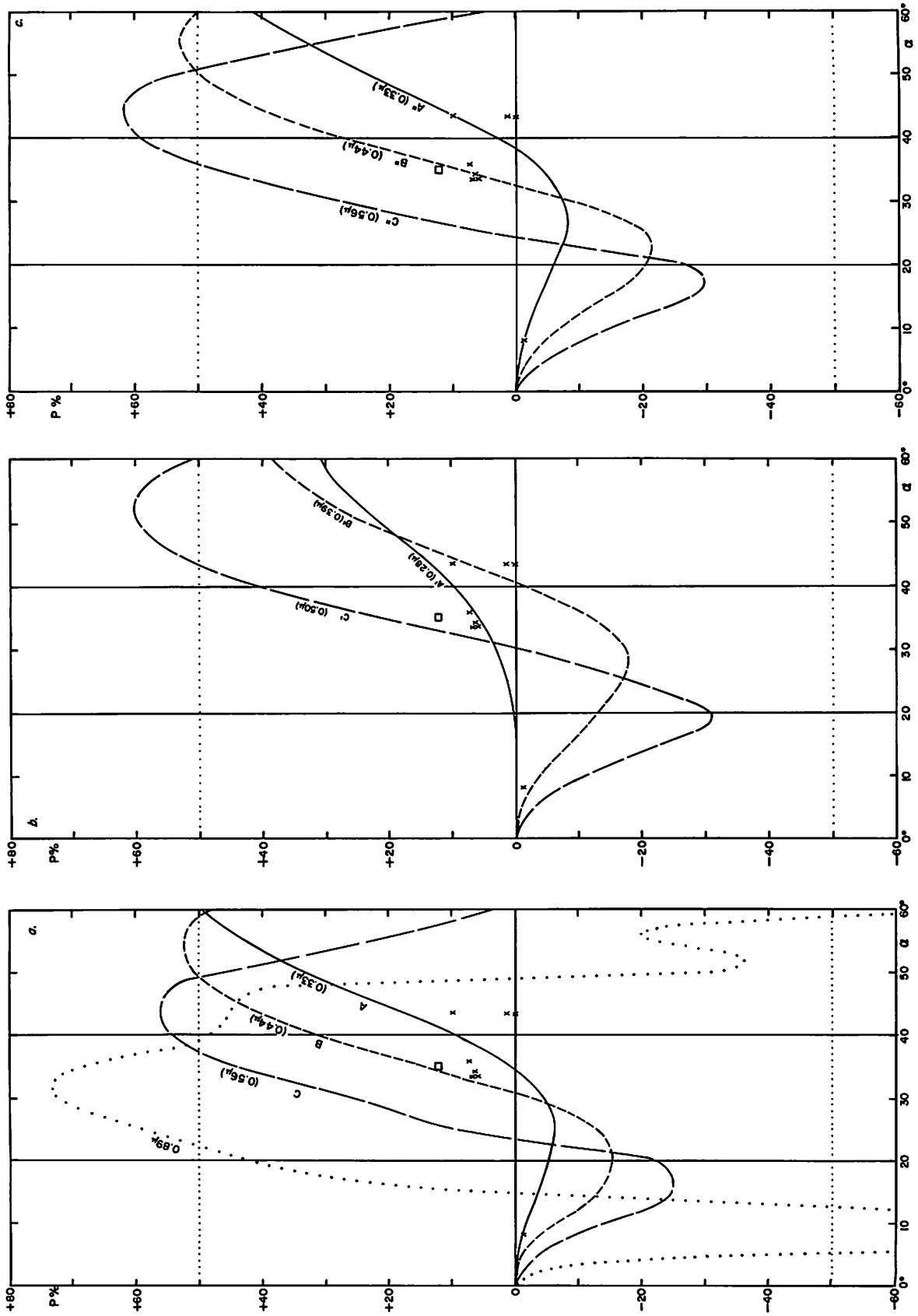

Fig. 3. Computed polarizations for three sets of mixtures of sub-micron ice spheres if observed at λ 0.35 μ, with available polarization measures entered (Gehrels, Teska, 1962) (cf. Table 3); (*a*) mixtures centered on integral values of scattering parameter, (*b*) mixtures centered on half-integral values, (*c*) "balanced" mixtures (see text).

pheric Physics, University of Arizona, for discussions on this general topic; this section depends largely on data and references he has supplied.

The atmospheric dust content will be a balance between (a) injection into the atmosphere and (b) elimination by free fall or scavenging by condensation products, which in the case of Mars must be limited to ice crystals. Evidence for such crystals, in addition to the haze and cloud phenomena already reviewed, is found in the presence of cloud caps over the poles in winter (cf. de Vaucouleurs, 1954, Sec. 47; Dollfus, 1961, p. 376). The crystals in these clouds may contain silicate condensation nuclei as do most terrestrial snow flakes. Ice deposited onto atmospheric dust could be responsible for the *variable transparency* of the general haze near $\lambda = 0.45\ \mu$, the "blue clearings" (Slipher, 1962), which appear to involve a temporary reduction in average particle size by perhaps 10 percent. This reduction could occur through a general temperature rise, or subsidence of an upper tropospheric air mass to the lower unsaturated zone; or else through a comparatively dust-free polar air mass moving into lower latitudes.

The elimination of atmospheric dust by free fall is governed by Stokes's law

$$V = \frac{\rho g d^2}{18\,\eta} \qquad (1)$$

(ρ = particle density; g = gravity; d = diameter; η = coeff. of viscosity) for the particles considerably larger than the mean free path in the Martian atmosphere ($d > 10\ \mu$); and for smaller particles by the Stokes-Cunningham law

$$V = \frac{\rho g d^2 (1 + k\lambda/d)}{18\,\eta} \qquad (2)$$

(λ is the mean free path; k a numerical factor of the order of unity). This law allows for the increased terminal velocity resulting from the discontinuities in the gaseous medium.

Dr. McDonald has kindly allowed the writer to quote from his computations of the terminal velocity as a function of d made for $\rho = 1$ and $g = g$ (Earth). They extend over the range $0.02\ \mu \leq d \leq 20\ \mu$ and a large range of atmospheric densities. For silicate particles on Mars the product $g\rho$ will be the same as used in McDonald's computations; they are reproduced in Table 4 for the range of atmospheric densities likely to be of interest. The three values of the pressure correspond to the levels 20 km, 30 km, and 40 km in the terrestrial atmosphere. (The temperature differences between the terrestrial stratosphere, ~220°K at 30 km, and the Martian troposphere are unimportant.)

TABLE 4

TERMINAL VELOCITIES OF SILICATE PARTICLES IN MARTIAN ATMOSPHERE
(Courtesy Dr. J. McDonald)
(V in cm/sec)

d (μ)	V for 55 mb	V for 11 mb	V for 2.7 mb
0.02	0.0002	0.001	0.004
0.10	0.0011	0.005	0.02
0.20	0.0024	0.011	0.04
1	0.014	0.06	0.2
2	0.033	0.12	0.4
10	0.5	0.8	2
20	1.7	2.5	5

It is seen that for large particles (20 μ) the terminal velocities indeed approach Stokes's law, which makes V independent of the gas density. For particles with $d \simeq 0.2\ \mu$, which could be partly responsible for the violet haze, there is a first-power dependence on gas density or pressure; but the rate of fall is so slow that a precise knowledge of atmospheric circulation would be needed to derive any conclusions: for 11 mb pressure, these particles fall 1 km in 10^7 seconds or 4 months; and 10 km (probably a representative height for this layer) in 3 years. Thermal convection and the annual circulation of the atmosphere could retain these particles in the atmosphere almost indefinitely.

The elimination of dust by rain in the *terrestrial* atmosphere has been investigated by Greenfield (1956). He finds that particles between about 0.1 and 10 μ have the lowest probability of being swept up. McDonald (1964) has emphasized the reasons: particles with $d >> 10\ \mu$ have so much inertia that rain drops collide with them and sweep them up. The very small particles ($d << 0.1\ \mu$) collide with droplets also, in this case because of their Brownian motion. This leaves the intermediate group for which the Brownian motion is small and the inertia also small, so that the particles are carried with the aerodynamic flow past the droplets.

Because of the very low frost point (around –78°C, see section 4) it cannot rain on Mars. Furthermore, at the very low Martian temperatures, the ice crystals settling over the polar caps are presumably platelets or prisms 1-10 μ in size rather than large, complex snowflakes (Fletcher, 1962, p. 259 ff). Therefore, the principal scavenging process will not be particle collison but rather *deposition of ice on silicate particles* that subsequently

fall, e.g., on the polar caps. The optical properties of the Martian polar regions through their annual cycle may give some indication of the degree of particle depletion there during the Martian winter.

The second aspect, the production and *atmospheric injection* of dust, is a process widely studied for the Earth. Reference is made to four monographs: *Micromeritics* (Dallavalle, 1948), *Particulate Clouds* (Green and Lane, 1957), *Air Chemistry and Radioactivity* (Junge, 1963), and *The Mechanics of Aerosols* (Fuks, 1955). It appears that the size-frequency curves of aerosols are usually normal gaussian error curves in log d; but the data are not always sufficient to show whether this law holds for all particles in the atmosphere or merely the part collected by special devices. Fletcher (1962, pp. 68-69) considers that the observed low frequency of dust particles with $d \leq 0.1\ \mu$ is real, because such particles are difficult to produce. Dr. McDonald further points out that even after dust particles are produced by grinding action (wind erosion) they will tend to stick to larger particles because natural aerodynamic gradients are far less than the surface-contact forces. Therefore, it is probable that also on Mars the injection of particles with $d < 0.1\ \mu$ is inappreciable.

With dust present in the Martian atmosphere its particles will act as active nuclei for the deposition of ice as soon as the temperature falls below the local frost point. The largest silicate particles will statistically be the most suitable hosts because they have the largest probability of presenting an area of sufficient size and with the proper lattice constant for attachment of an ice embryo (Fletcher, 1962, p. 210 ff.). Physically, this process can occur for temperatures below about –20°C, depending on the composition of the dust (*op. cit.* pp. 245-250). As is true for the Earth, meteoritic dust will make a contribution to the total dust content (*op. cit.* pp. 250-258).

The growth rate of the ice crystals is given by

$$\frac{dM}{dt} = \text{const.}\, r\,(n_o - n_c), \tag{3}$$

in which M is the mass of the particle, r its radius, n_o the concentration of vapor molecules at a distance and n_c the concentration at the crystal surface (Fletcher, *op. cit.*, p. 266). If relative effects of ventilation are neglected ($n_o - n_c = \text{const.}$) it follows that

$$r = \text{const.}\, \sqrt{(t - t_o)}, \tag{4}$$

in which the constant may be positive, zero, or negative depending on the sign of $(n_o - n_c)$; n_c depends on T and the nature of the surface. Partly because of the latter factor, a forecast on the steady-state distribution of diameters of the very small ice crystals in an atmosphere with exceedingly low values of n_o and n_c is not readily made. The effect of surface curvature will tend to favor the larger ice crystals, but those well above 1 μ will fall out from the haze layer (cf. Table 1) and evaporate in the lower, unsaturated parts of the atmosphere. A cloud with rather uniform particle diameters may therefore result, and may account for the blue-violet haze layer actually observed. Because of atmospheric circulation and subsidence of air masses, inhomogeneities in the haze layer will be expected. Conversely, the *circulation of the Martian atmosphere will in principle be accessible to systematic study from the Earth through a continuous patrol by UV photography and polarimetry with the highest possible resolution.* A constant component might be detected that would be molecular, leading to an independent determination of the atmospheric gas content.

The repeated falling out of the largest ice crystals from the haze layer means that in the steady state the water-vapor mixing ratio of the lower troposphere will be larger, and clouds with increased crystal size within the haze layer can be formed by convective updraft from below. The frost deposits on the polar areas and their periodic evaporation at ground level will have a similar enriching effect. In this manner a "lumpy" pattern as observed on the UV photographs can be accounted for.

An interesting question concerns the *electrical* state of a Martian dust cloud. Experience with conditions of extremely low humidity on the Earth, such as are found in the Sahara Desert, indicates the possibility of large electrical gradients in dust clouds and frequent small lightning discharges.

The atmospheric density cannot be found with precision from the mere occurrence of dust storms. At the McDonald Observatory I have observed particle sizes in terrestrial dust storms by collecting the dust on exposed sticky surfaces (glass, coated with oil), 10-15 meters above the ground. It was found, among others, that for 20 miles-per-hour (9 meters-per-second) winds, the dust ranged in size up to 25 μ diameter. The "gustiness" of the wind, expressed as the vertical rms velocity, is about 0.1 of the horizontal wind speed, or $\pm$ 0.9 mps, whereas on the Earth the rate of fall of a 25 μ particle of $\rho = 2.5$, according to Dr. McDonald's table, is 0.05

mps. The ratio of 1/18 must represent the net ascent of dust-laden air near the surface in an otherwise near-random process. For Mars winds of similar magnitude (4-10 mps, Antoniadi 1930, pp. 45-46) have been derived from moving cloud masses; Martian dust storms may require double this speed or more.

If an 18 meter-per-second (40 mph) wind is assumed as typical for a Martian dust storm and the surface pressure were 10 mb, the aerodynamic force per unit area on the dust would be ρV^2 or 1/20 of the force acting on the terrestrial dust referred to. Particles of 25 $\mu/20 = 1.25$ μ would then be carried away on Mars, which is not inconsistent with the observed yellowish color of the dust; though, for the assumed wind velocity, *the pressure could not be much less or the particles raised would not be yellow.* The rate of fall of such particles would be about 0.07 cm per second (see Table 4) so that the dust could stay in a quiet atmosphere for 1-10 days, not inconsistent with the observations.

As Mr. T. Owen has pointed out to the writer, there is an alternative mechanism for the injection of dust into the Martian atmosphere: *dust devils.* In terrestrial deserts these are frequent and their dust columns are often visible to heights of 1-2 km, particularly when viewed in polarized light normal to the sun. The heating of the Martian soil in a sky almost always perfectly clear must be conducive to the formation of dust devils. They cannot, of course, be responsible for the massive dust clouds referred to above.

The discussion of Section 2 sets an upper limit to the molecular content of the Martian atmosphere; that of Section 3 a very rough lower limit. Taken together an atmospheric pressure around 10-20 mb appears plausible. The limits can be sharpened by further work, and UV polarization measures and photometry should yield an actual value of, not merely a limit to, the molecular scattering power.

4. The Spectral Records

The infrared spectrum of the planet yields data on both the atmospheric composition and the pressure more specific than do the data on atmospheric scattering.

The spectrum from 1-2 μ was observed in 1947 with resolutions $\lambda/\triangle\lambda$ of about 80, which led to the discovery of CO_2 in the atmosphere. "The bands near 1.6 microns were three times as strong in the Mars spectrum as in the Moon spectrum taken at the same altitude. Spectra of the Sun at different altitudes confirm this conclusion. Because of pressure effects on the band intensity, the CO_2 content of the Mars atmosphere will actually be somewhat larger than that of the Earth if the total pressure on Mars is less than on the Earth, as is likely. No other gases having strong infrared absorptions, like CH_4, NH_3, or N_2O were found. They could not be present except in exceedingly small quantities" (Kuiper 1947). The CO_2 bands recorded were the (strong) central pair of the tetrad (301, 221, 141, 061) near 1.6 μ. In 1948 the somewhat stronger triad (201, 121, 041) was observed also (Kuiper 1949, p. 335), with intensities roughly consistent with the 1.6 μ group.

Further, the Martian polar caps were observed and found to exhibit the reflection spectrum of H_2O snow, not CO_2 snow (*op. cit.*, pp. 336-337). From the gradient of the reflection curve near 2 μ it was found that the ice crystals of the polar caps were much smaller than in terrestrial snow, but were nearly matched by frost deposited on dry ice.

In the first part of the 19th century it was generally held that the maria on the planet were genuine seas. This concept was challenged by Kaiser (1872), who however offered no substitute explanation. Liais and Cruls (1878) and Trouvelot (1884) were the first to hypothesize that the dark areas were vegetation. The assumption that the snows of the polar caps "melted" at 0°C continued to be made, however (except by authors who supposed the caps to be frozen CO_2). It is true that the measured temperatures of the caps were much below 0°C, but Coblentz (1926) attributed this to Martian atmospheric absorption. The writer (1931), comparing the measured Martian temperatures with data on water vapor then available (the Mt. Wilson measures of 1925), concluded that the frost point on Mars was about −56°C and that no free liquid water can exist on the planet; only ice and water vapor. Since the water-vapor data were marginal, the actual frost point could be lower. A better determination was made from the extent of the polar cap, on the assumption that the theoretically-computed temperature at its boundary represents the frost point (Kuiper 1952, p. 389); and from the presence of ice particles in the Martian atmosphere at temperatures that may be estimated. In this manner $T_f = -78$°C was derived, with an upper limit of −73°C; and the total amount of precipitable water in the Martian atmosphere of the order of 8 μ (for the upper limit of −73°C the corresponding amount is 18 μ).

Grandjean and Goody (1955) computed the atmospheric CO_2 abundance from Kuiper's observations of the 1.575 and 1.605 μ bands on the assumption that $p = 100$ mb. Sinton (1961) published low-resolution spectra of Mars and the moon taken in 1954, indicating the presence of the 10-12 μ bands of CO_2; Weaver *et al.* (1963) announced the observation from a balloon of the 2 μ bands of CO_2 merged as one feature and computed the upper limit of Martian water vapor to be 40 μ; while Dollfus (1963, 1964) attempted to observe Martian water vapor near 1.4 μ by using narrow-band filter photometry at the Jungfraujoch and found 150 μ of H_2O. An excellent high-dispersion spectrum taken in the 0.8-0.9 μ region with the Mt. Wilson 100-inch coudé spectograph by Spinrad, Münch, and Kaplan (1963, 1964) recorded Doppler-separated Martian H_2O at 0.82 μ and CO_2 at 0.87 μ. They found 14 ± 7 μ of H_2O, confirming the estimate from the size of the polar cap but contradicting the high value derived by Dollfus.

5. *McDonald Spectra, 1962-63 Opposition*

Spectral records for the 1-2.5 μ region were obtained with the 82-inch telescope during the past several oppositions, but those taken in December 1962 - January 1963 are the most complete and have been extensively calibrated in the laboratory. These Mars spectra are reproduced here, together with lunar and some preliminary laboratory comparisons. The more definitive laboratory calibrations of CO_2 are found in *Communications* No. 32 by Owen and Kuiper; and those of trace constituents in *Comm.* No. 34 by Kuiper and Cruikshank. A preliminary account of the spectra was presented at the Liège Conference, June 1963 (Kuiper 1963).

The smallest slit width used in the Mars records is 0.3 mm (2 seconds of arc at the Cassegrain focus) which results in resolution $\lambda/\triangle\lambda$ of about 1000 and $\triangle\lambda = 0.001$-0.002 μ. In the photographic infrared (0.75-1.1 μ) photographic spectra with much higher resolution have been obtained at Mt. Wilson and elsewhere but a few rapid-scan records (0.01 μ or 100Å per minute) with the same medium resolution as used beyond 1 μ are included here for comparison purposes. These records are shown in Figures 4 and 6, with Figures 5 and 7 showing lunar comparisons taken on the same night. The lunar image on the slit was thrown far out of focus to reduce spurious intensity changes in the spectra resulting from the drift of the lunar image over the slit; even so, the lunar comparisons had to be run faster and have somewhat reduced resolution. The atmospheric humidity was only about 1 mm precipitable water in the overlying atmosphere but still too high to show the Martian water vapor directly.

In Figure 8 the record is extended to 1.4 μ; the scanning rate was again 0.01 μ per minute. The lunar comparison in Figure 9, taken at 0.05 μ per minute, has somewhat less resolution and less electronic noise. Figure 8 shows the (103) and (023) bands of CO_2 at 1.20 and 1.22 μ, and marginally, the (241) band at 1.32 μ. These may be compared with the laboratory bands shown in Figure 14. The Martian 1.2 μ bands, (103) and (023), have on the basis of Figure 8 and 9, equivalent widths of 2.0Å and 1.3Å, respectively. In the laboratory comparison shown in Figure 14 the widths are 3.1Å and 1.9Å, respectively.

Figure 10 is the first record obtained during the past opposition of the 1.4-1.8 μ region, with Figure 11 serving as a lunar comparison for it as well as for Figure 12.

On the dry night, December 8, 1962, three records of the 1.4-1.8 μ region were obtained which are shown in Figure 12; the top graph is not a direct trace, but the average of the two lowest traces, which had a shorter time constant (5.5 seconds) than the third (11 sec) and show, therefore, more electronic noise. The top graph will therefore have an intrinsic noise comparable to the $\tau = 11$ sec trace placed just below, but have somewhat increased resolving power. The upper two graphs are independent of one another and together contain the substance of Figure 12. It is seen that they define the Martian 1.6 μ tetrad of CO_2 moderately well. Figure 13 shows two additional scans, obtained mid-January 1963, with a laboratory trace added for purposes of identification. Figure 14 serves the same purpose for the Martian records of Figure 12.

Planimeter measurements of the two strong bands at 1.6 μ on Figure 12 show the equivalent width of the Martian plus telluric CO_2 absorptions to be 1.20 times as large as that of the laboratory comparison, which is 80 meters of CO_2 at $p = 17$ cm or 18 m atm. The telluric components may be subtracted with the aid of Figure 11. The equivalent widths of the 1.575 and 1.605 μ bands average 12.8Å on Figure 11 and 27.6Å on Figure 12. On December 8, 1962, Mars was receding from the sun at a rate of 1.65 km/sec and approaching the Earth at a rate of 13.65 km/sec. Hence the Martian CO_2 bands were displaced corresponding to -13.6 km/sec or by -0.72Å. The Michigan Atlas of the

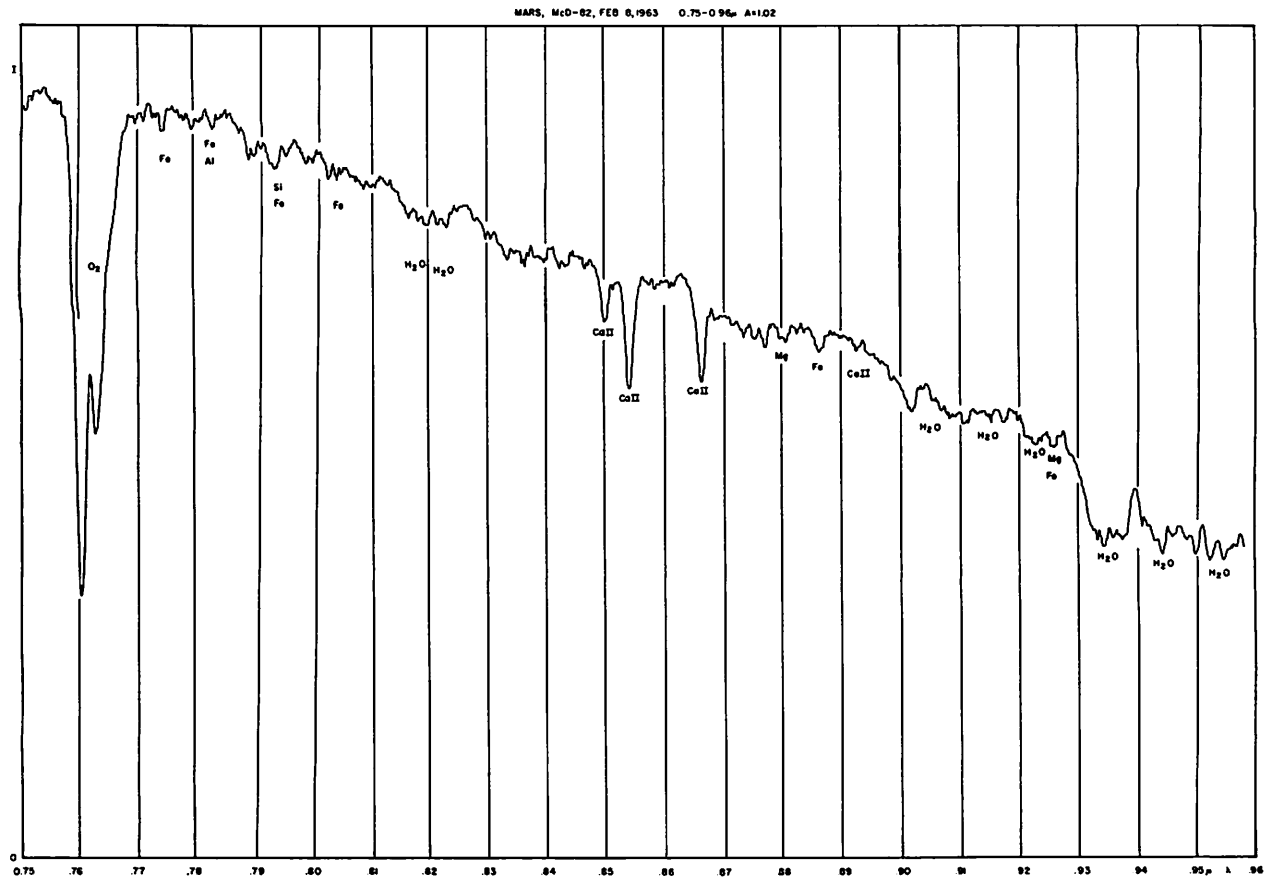

Fig. 4. Mars, equatorial strip, 0.75-0.96 μ, McDonald Observatory, February 8. 1963; T = 52° F, relative humidity (H) = 0.34, declination (Dec.) + 21°1, hour angle (H.A.), 0^h21^m-0^h31^m W, air mass 1.02; Dumont S-1 photomultiplier, grating 1.0 μ, RG 8 filter, entrance and exit slits both 0.25 mm, scanning rates 12.5/0.5, time constant (τ) = 1 sec.

solar spectrum (Mohler, *et al.*, 1950), small sections of which are reproduced in Figure 16, shows that for the two bands in question the Martian and telluric CO_2 lines will have been completely separated. (The separation is somewhat larger than shown because instrumental broadening in Fig. 16 is about 0.5Å.) Since the two bands are each about 0.02 μ = 200Å wide, the average telluric absorption is 6.4 percent and the reference continuum of the Mars absorption may therefore be regarded to be depressed by this amount. The average equivalent width of the Mars bands on December 8 was therefore (27.6–12.8)/0.936 = 15.8Å.

The observed Martian spectra are a blend of solar, telluric, and Martian absorptions. The calibration of these spectra would therefore best be made by channeling natural sunlight, received through the Earth atmosphere, through an absorption tube that simulates the Martian atmosphere; though one cannot reproduce this way the apparent radial velocity of the planet.

Mr. T. Owen has succeeded in obtaining such composite spectra. Only the 2-meter tube (allowing an 80-meter total path length) was available at the time the bulk of this paper was prepared and the numerical comparisons must still allow for the pressure difference, Mars-laboratory, at the point of intensity match. It was found from records such as shown in Figure 15 that p = 11 cm (11.5 meter atm of CO_2) well represents the Martian spectrum. Improved comparisons made with the long absorption tube are found in *Comm.* No. 32.

The Martian spectral record is continued to 2.5 μ in Figures 17, 19 and 20, with Figure 18 giving three lunar comparisons and Figure 21 laboratory comparisons. The matching of the curves of Figure 21 with the 2 μ CO_2 absorptions of Mars leads to a similar result as discussed on the basis of Figure 15.

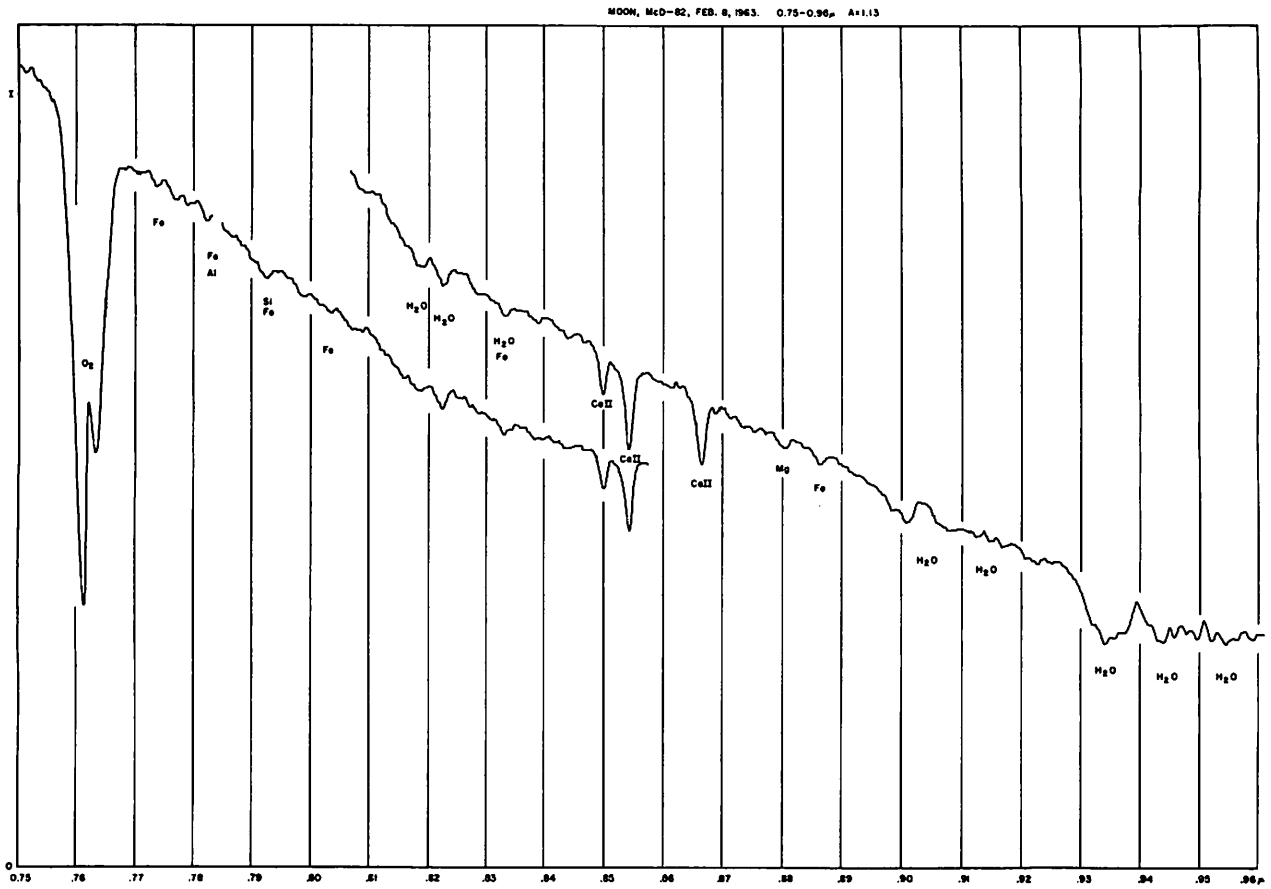

Fig. 5. Moon comparison for Figure 4, 0.75-0.96 μ, February 8, 1963; T = 52° F, H = 0.34, Dec. + 17°1, H.A. 1^h42^m-1^h52^m W, air mass 1.13, Cell S-1, grating 1.0 μ, RG 8 filter, slits 0.25 mm, scan 12.5/0.5, τ = 1.0 sec.

6. *Gases Other Than* $C^{12}O_2^{16}$

The λ 0.87 μ band observed at Mt. Wilson allows a determination of the Martian CO_2 abundance; this subject is treated by Mr. Owen in *Comm.* No. 33 on the basis of two new calibrations. The spectra here reproduced allow, upon calibration, a determination of the atmospheric pressure and an estimate of the total quantity of constituents other than CO_2 (*Comm.* No. 32 by Owen and Kuiper). There remains to examine direct spectral evidence for both constituents other than CO_2 and isotopic bands.

Only one CO_2 *isotopic band* is distinctly visible, λ 2.15 μ of $C^{12}O^{16}O^{18}$ (Figures 17 and 19). The boundaries at 2.14 and 2.18 μ shown in Figure 17 were taken from the much stronger Venus absorption (*Comm.* No. 15). The profile is disturbed by the solar hydrogen line B7 whose equivalent width was found to be 1.8Å from the records of the Michigan Atlas and 3Å from Figure 18. With allowance for B7 the equivalent width of the 2.15 μ CO_2 band in Mars was from Figure 17 found to be 6.9 ± 1Å.

Laboratory calibrations were made at p = 6 cm and 12 cm, with path lengths 180, 360, 720, and 1440 meters. Two of the spectra are reproduced in Figure 22. The measured equivalent widths are listed in Table 5; each entry is based on two or three spectra.

TABLE 5

EQUIVALENT WIDTHS IN Å OF λ 2.15 μ ($C^{12}O^{16}O^{18}$)

PATHLENGTH	p = 6 cm	p = 12 cm
180 m.....	—	4.8
360 m.....	3.7	9.4
720 m.....	6.2	14.4
1440 m.....	8.65	22.5

The measures of Table 5 are plotted logarithmically in Figure 23a. The abscissae are the products of the abundance w (in meter-atm) and pressure p (in cm Hg); the ordinates are the equivalent widths (EW) in Å. The measures are well represented by

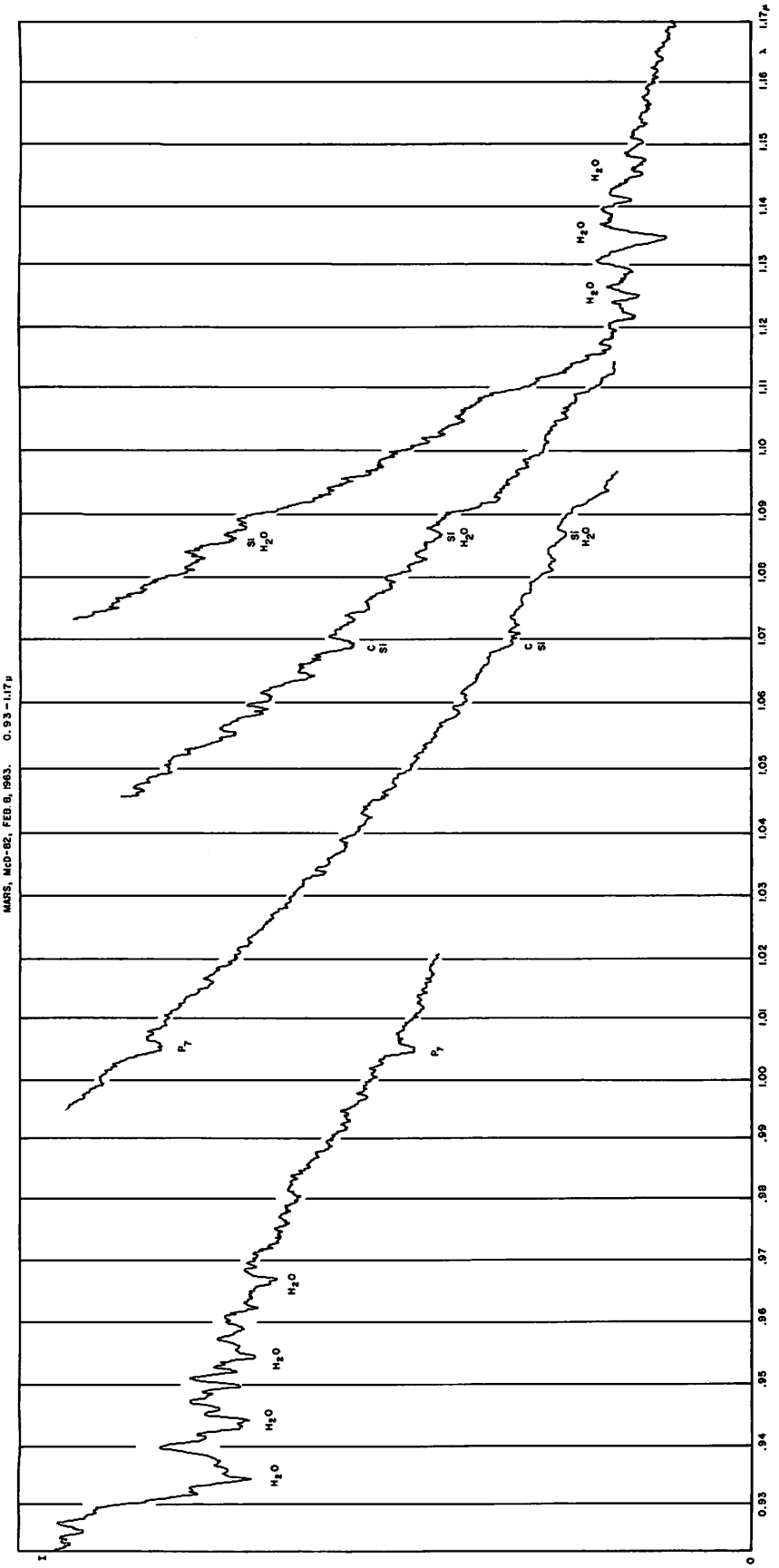

Fig. 6. Mars, 0.93-1.17 μ, February 8, 1963, overlapping scans with different gains. T = 51° F, H = 0.35, Dec. + 21°.1, H.A. 0^h14^m-0^h21^m W, Cell S-1, 1.0 μ grating, RG 8 filter, 0.25 mm slits, scan 25/1 or approximately 0.01 μ/min (two right-hand traces), 12.5/0.5 or 0.02 μ/min (two left-hand traces); τ = 2 sec and 1 sec, respectively.

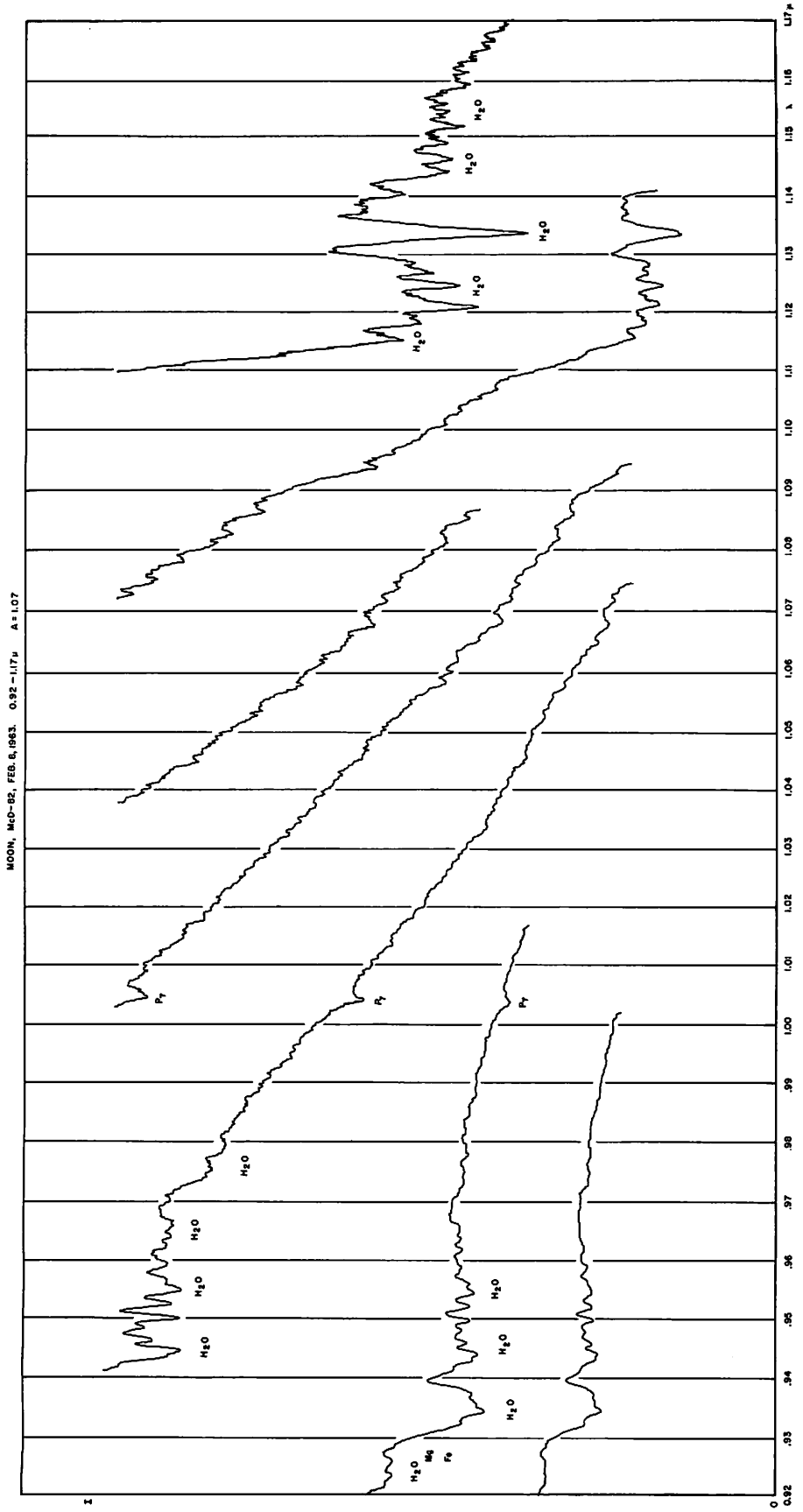

Fig. 7. Moon comparison for Figure 6, 0.92-1.17 μ, February 8, 1963, T = 51° F, H = 0.35, Dec. + 17°3, air mass 1.07, Cell S-1, grating 1.0 μ, filter RG 8, slits 0.25 mm, scan 12.5/0.5, $\tau = 1$ sec.

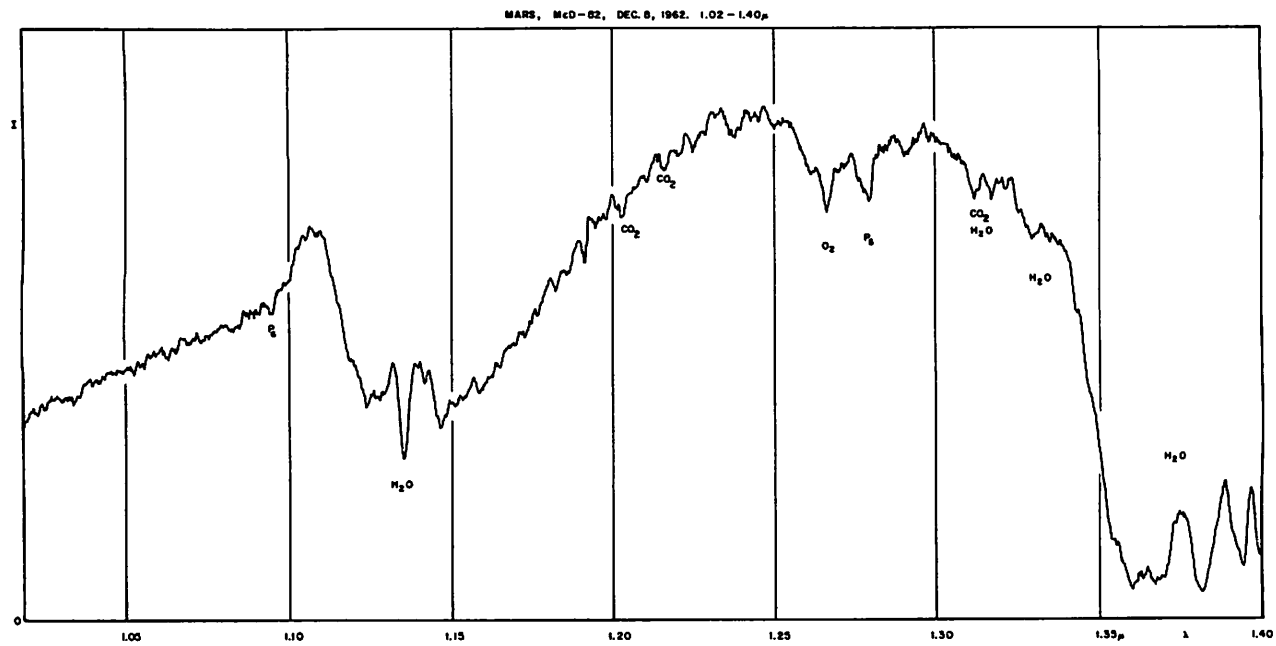

Fig. 8. Mars, 1.02-1.40 μ, December 8, 1962, T = 42° F, H = 0.55, Dec. + 16°4, H.A. 0^h12^m E - 0^h24^m W, 0.25 by 0.25 mm cell + Fabry lens, grating 1.6 μ, filter 2540 Corning, slits 0.7 and 1.0 mm, scan 25/2, τ = 5.5 sec.

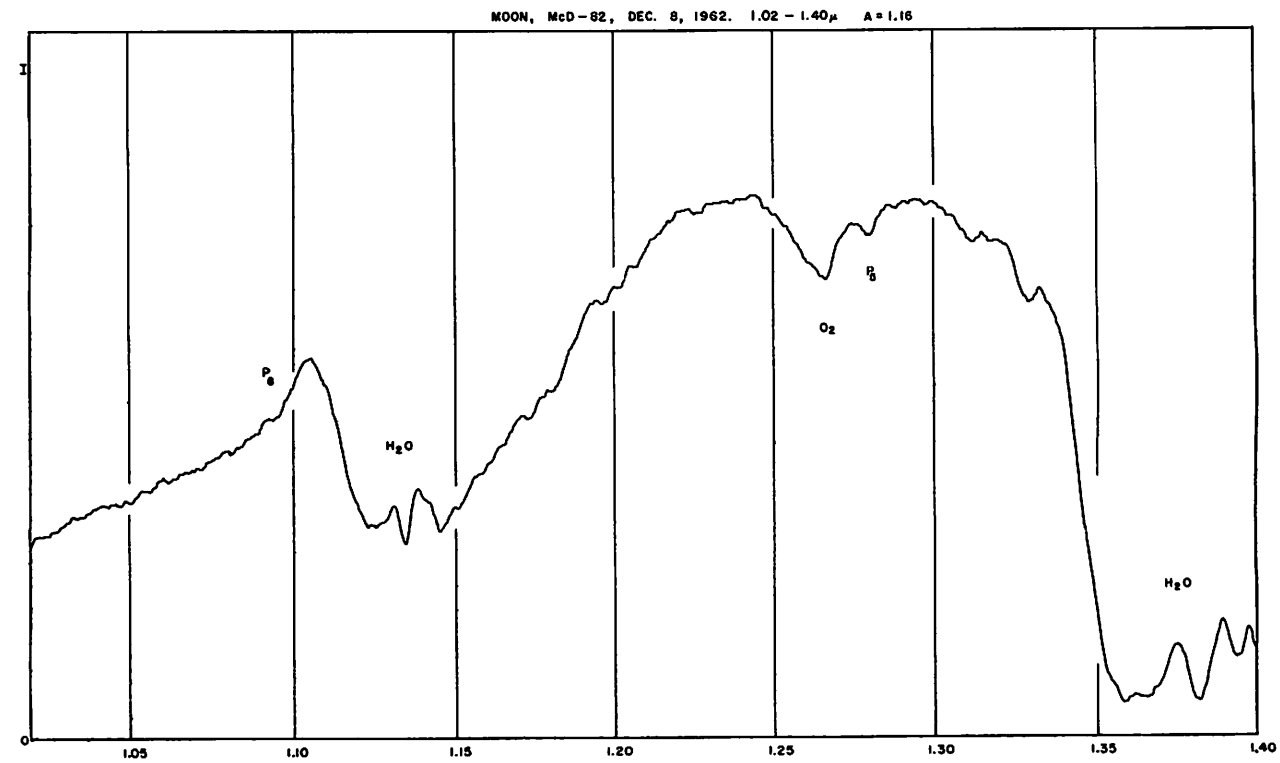

Fig. 9. Moon comparison for Figure 8, 1.02-1.40 μ, December 8, 1962, T = 42° F, H = 0.55, Dec. + 7°0, H.A. 1^h23^m-1^h30^m W, air mass 1.16, cell 0.25 by 0.25 mm + Fabry lens, grating 1.6 μ, filter 2540, slits 0.7 and 1.0 mm, scan 5/0.5, τ = 1 sec.

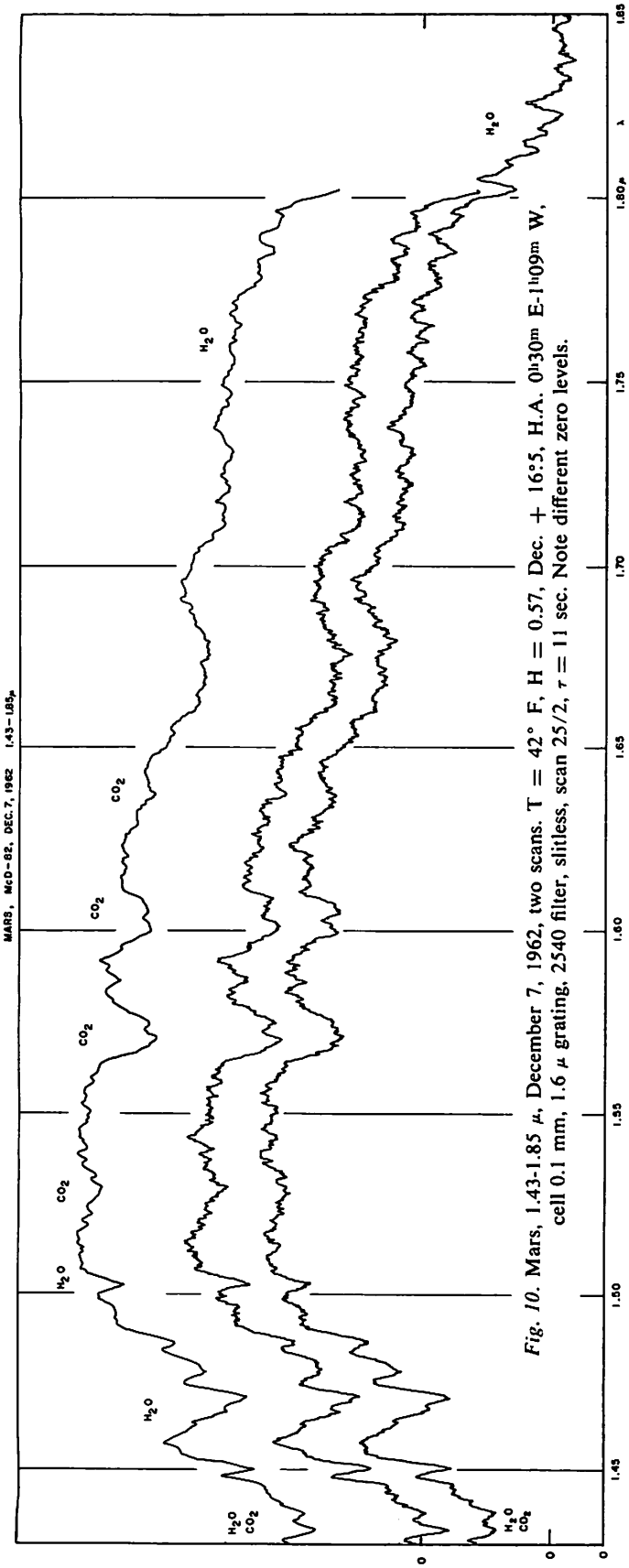

Fig. 10. Mars, 1.43-1.85 μ, December 7, 1962, two scans. T = 42° F, H = 0.57, Dec. + 16°5, H.A. 0^{h}30^m E-1^{h}09^m W, cell 0.1 mm, 1.6 μ grating, 2540 filter, slitless, scan 25/2, τ = 11 sec. Note different zero levels.

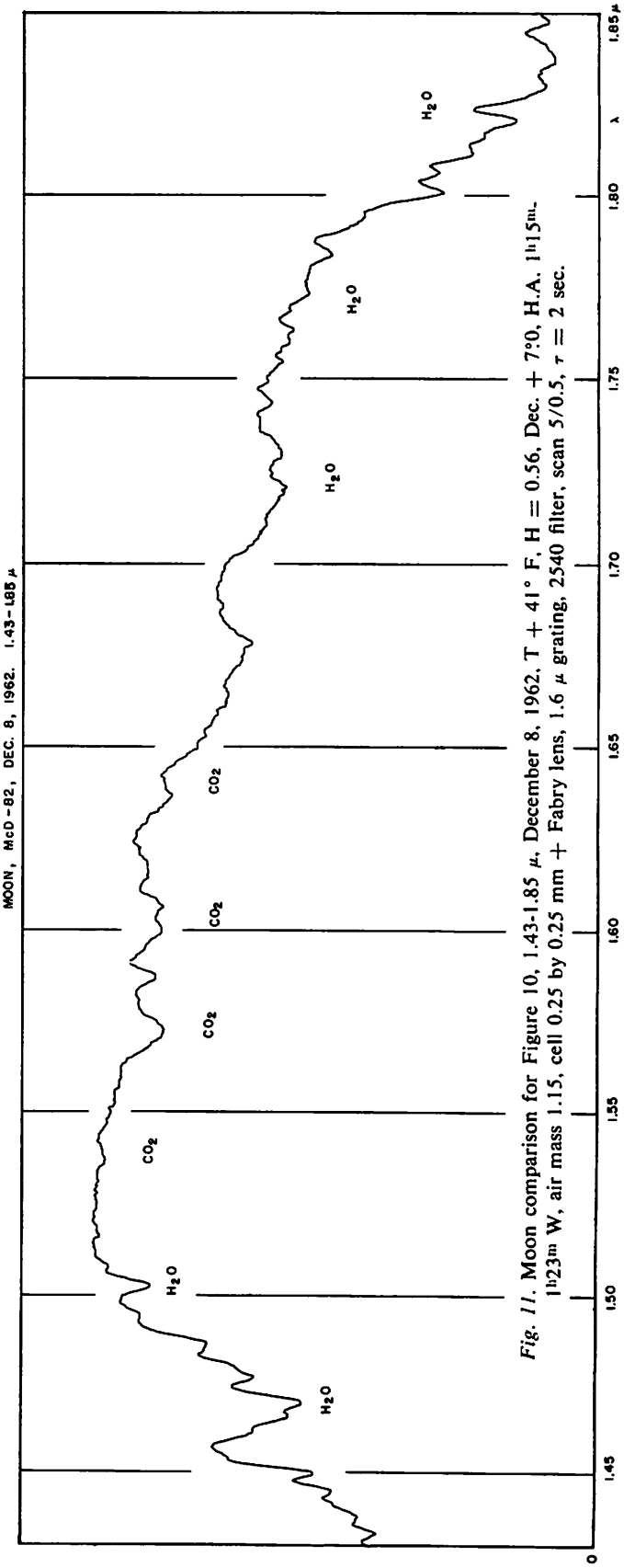

Fig. 11. Moon comparison for Figure 10, 1.43-1.85 μ, December 8, 1962, T + 41° F, H = 0.56, Dec. + 7°0, H.A. 1^{h}15^m 1^{h}23^m W, air mass 1.15, cell 0.25 by 0.25 mm + Fabry lens, 1.6 μ grating, 2540 filter, scan 5/0.5, τ = 2 sec.

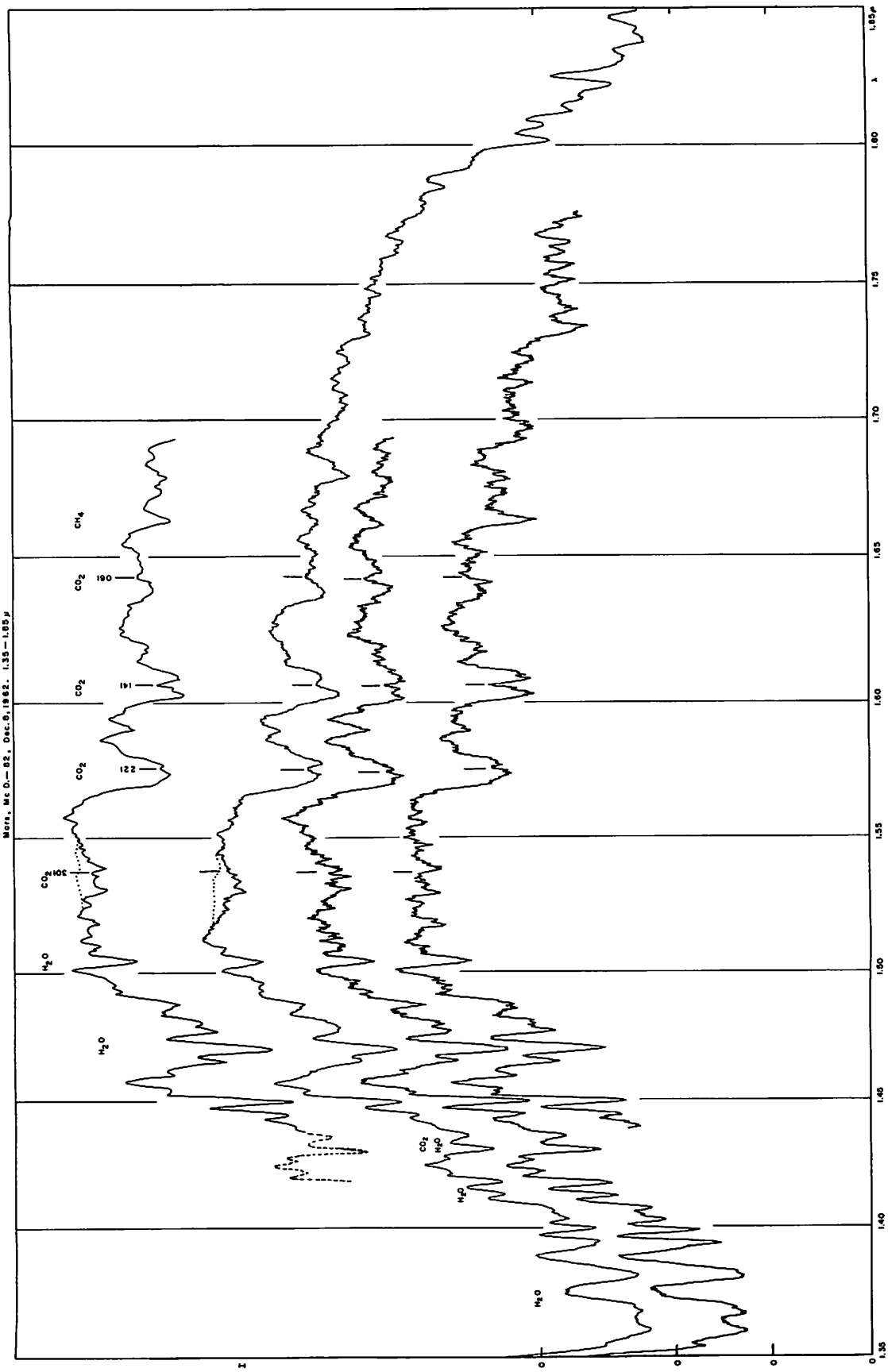

Fig. 12. Mars, 1.35-1.85 μ, December 8, 1962, three scans. T = 42° F, H = 0.55, Dec. + 16°4, 0.25 by 0.25 mm cell + Fabry lens, 1.6 μ grating, 2540 filter, slits 0.7 and 1.0 mm, scan 25/2. *Upper* spectrum: H.A. 1^h09^m-0^h19^m E (after this, Figure 8 was recorded), τ = 11 sec; *middle* spectrum: H.A. 0^h28^m-1^h02^m W, τ = 5.5 sec; *lower* spectrum: H.A. 1^h05^m-1^h38^m W, τ = 5.5 sec. Graph on top is *average* of two lowest (τ = 5.5 sec) scans.

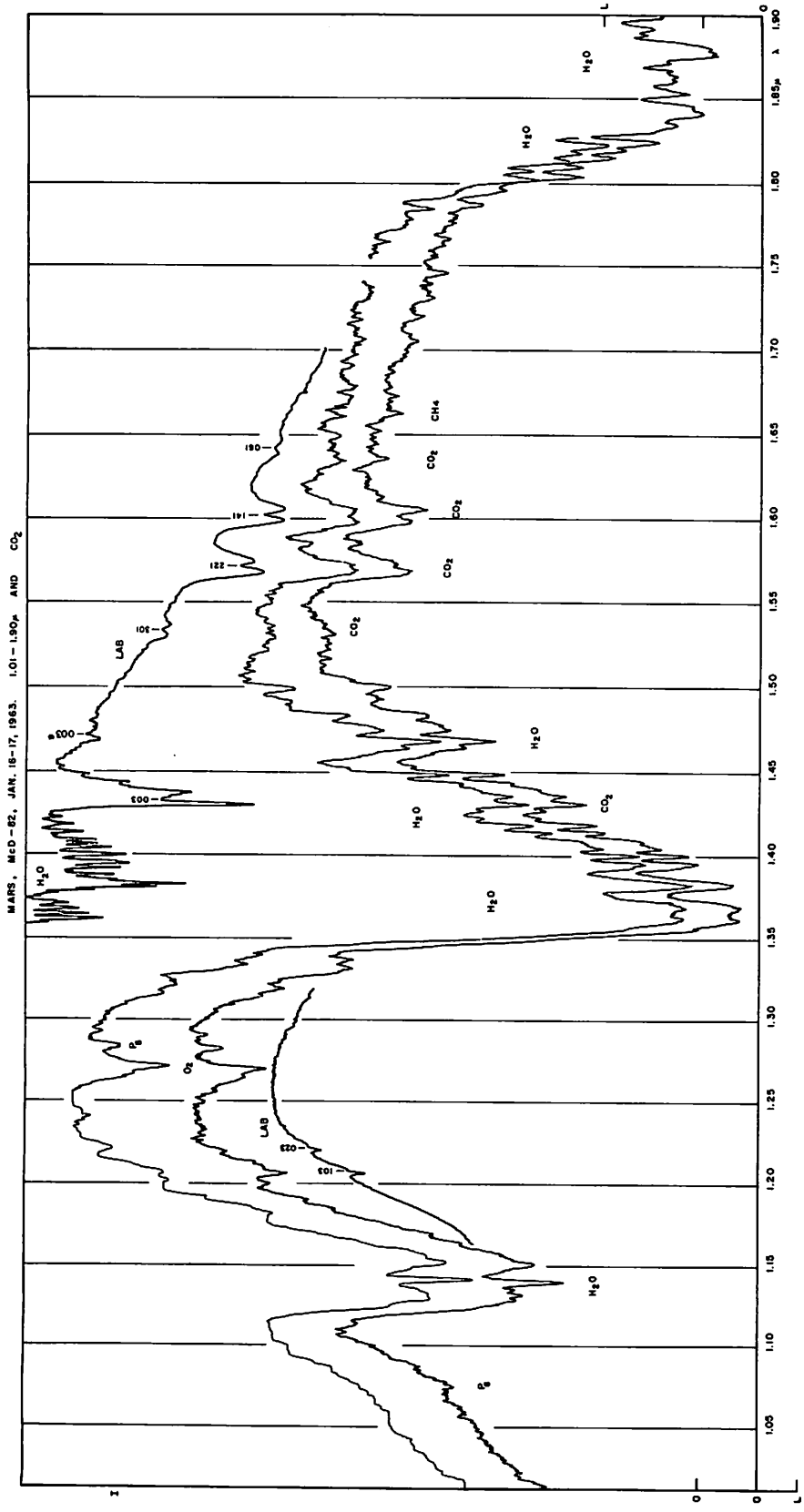

Fig. 13. Mars, 1.01-1.90 μ, Dec. + 18°3, two scans, cell 0.1 mm, 1.6 μ grating, 2540 filter, first slit 1.0 mm, scan 12.5/2. $\tau = 5$ sec. *Lower* spectrum: January 16, 1963, T = 33° F, H = 0.50, H.A. 2^h57^m-3^h40^m W. *Upper* spectrum: January 17, 1963, T = 39° F, H = 0.51, H.A. 1^h00^m-1^h40^m W. CO_2 for comparison, 80-meter path at $p = 17$ cm.

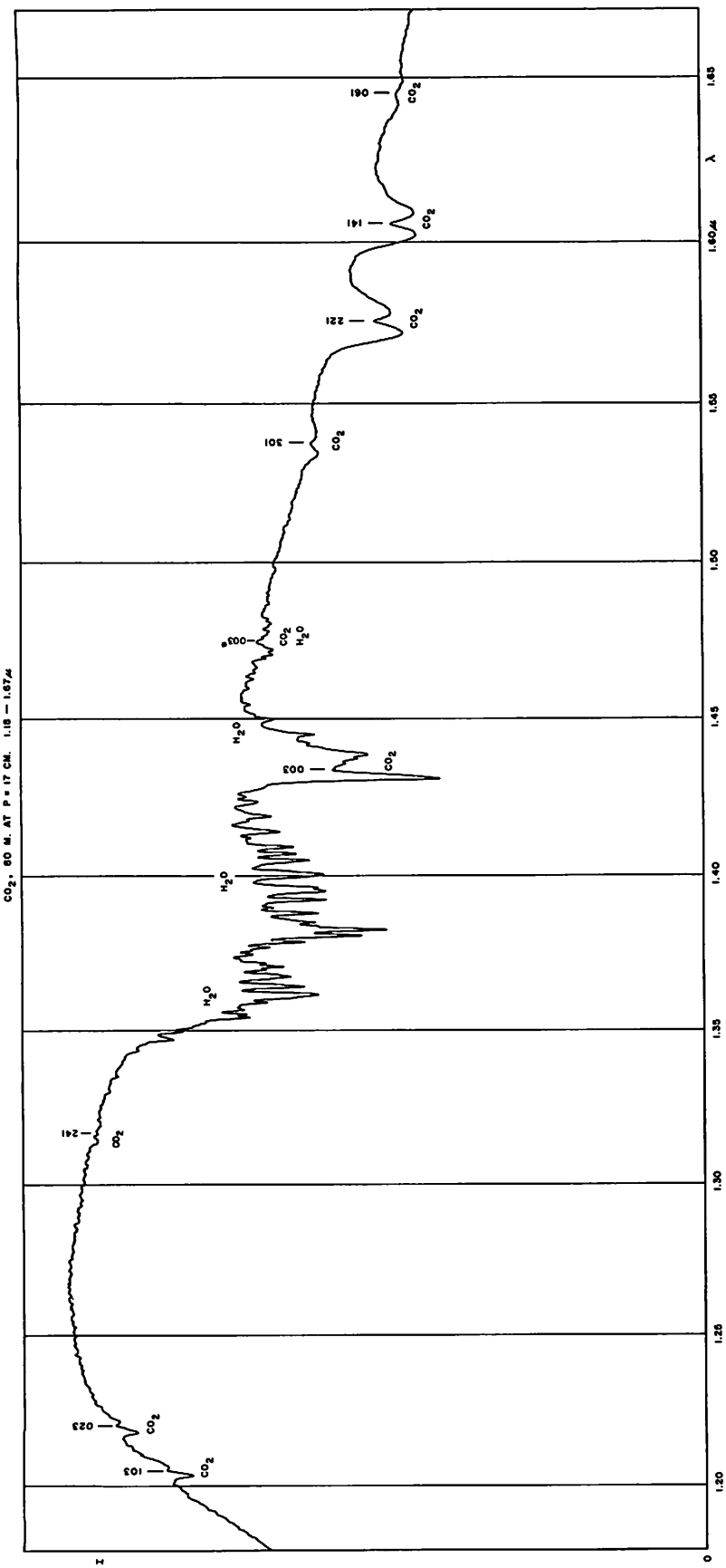

Fig. 14. Laboratory spectrum, 80 meters of CO_2 at $p = 17$ cm. Residual H_2O in laboratory and spectrometer, amount roughly 0.1 mm precipitable water; cell 0.25 mm, 1.6 μ grating, 2540 filter, slit 0.3 mm, scan 12.5/1, $\tau = 1$ sec.

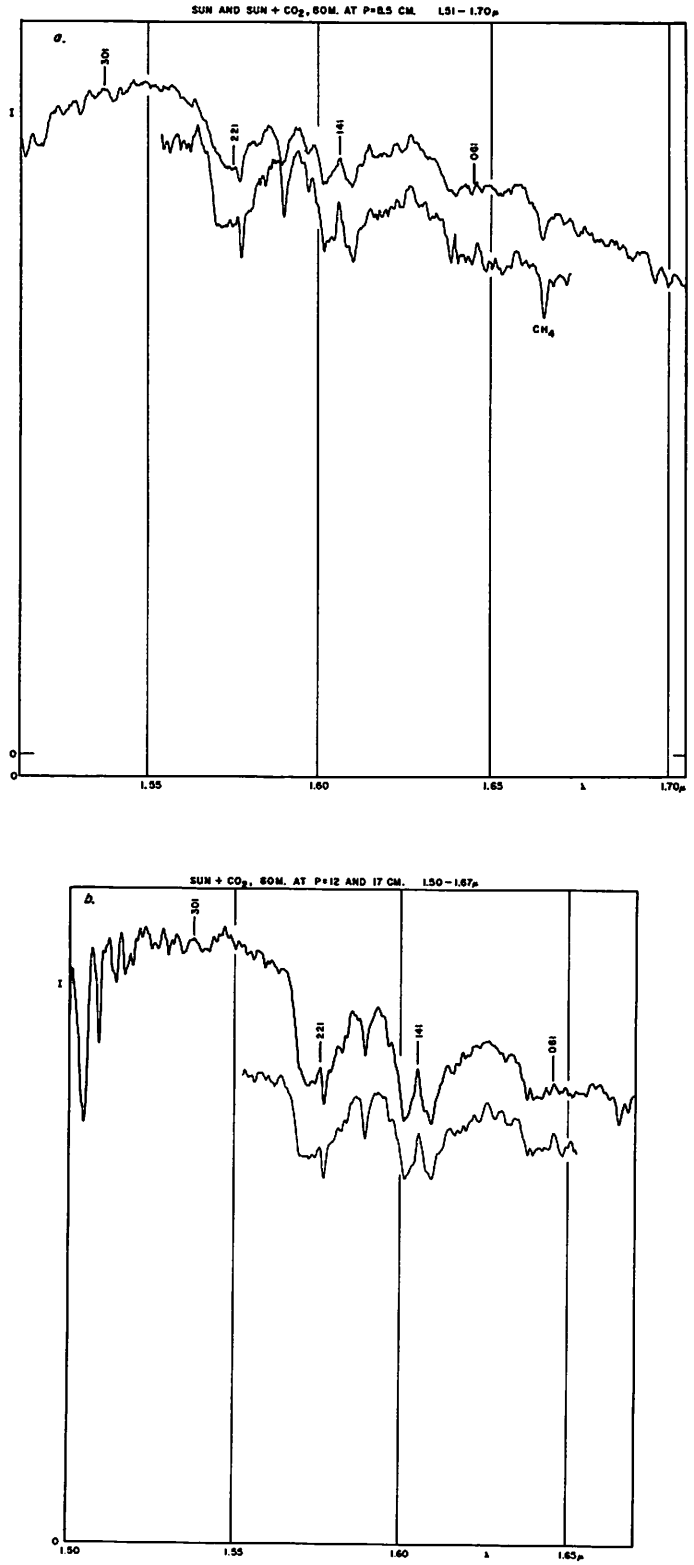

Fig. 15. Solar spectra, 1.50-1.70 μ, June 13 and 14, 1963, observed through 80 meters of CO_2 at $p = 0$, 8.5, 12, and 17 cm. for comparison with 1.6 μ Mars bands; 0.25 mm cell, 1.6 μ grating, 2540 filter, 0.3 mm slit, scan 12.5/1, $\tau = 1$ sec.

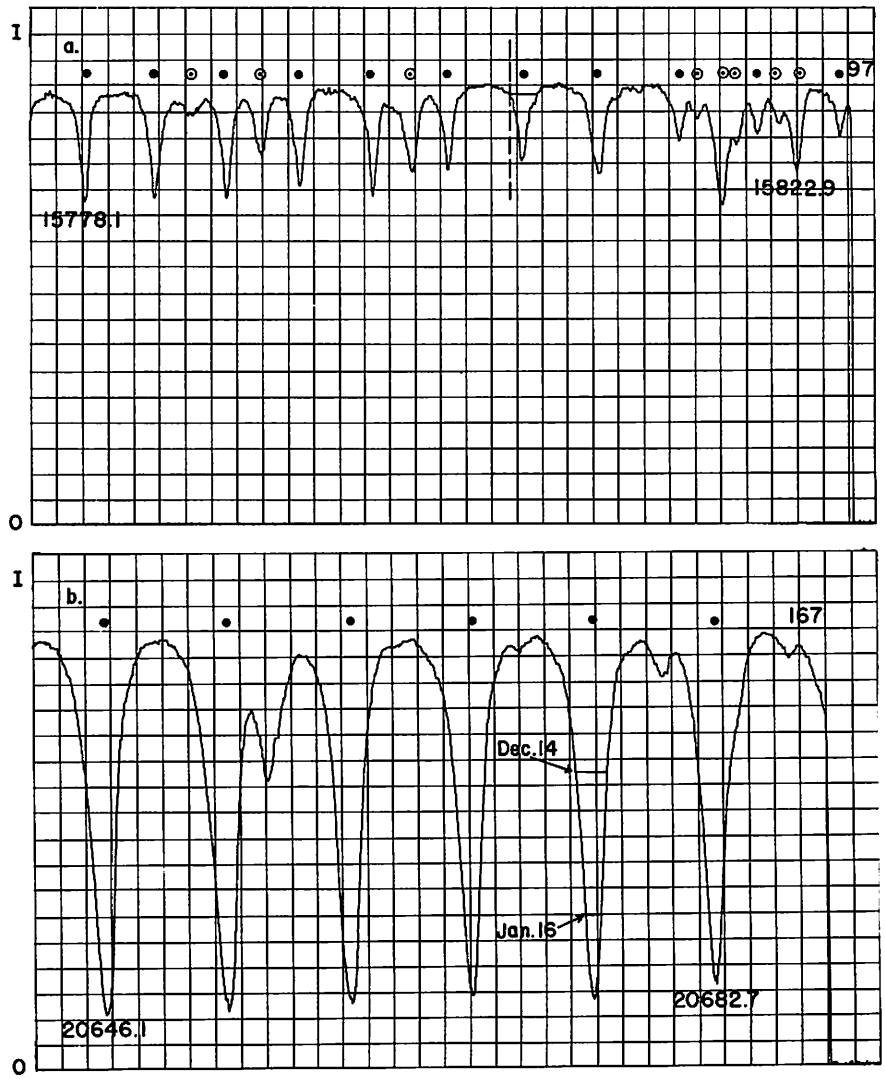

Fig. 16. Two small sections of Michigan Atlas of solar spectrum; dots signify telluric components. Displaced positions of Martian CO_2 lines indicated; (a) λλ 15775-15826 Å, Mars Dec. 8, 1962, V = −13.6 km/sec, Δλ = 0.72 Å; (b) λλ 20642-20689 Å, Mars Dec. 14, 1962, V = −13.2 km/sec, Δλ = −0.91 Å; and Jan. 16, 1963, V = −6.5 km/sec, Δλ = −0.45 Å.

Fig. 17. Mars, 1.90-2.50 μ, December 14, 1962, two scans. T = 40° F, H = 0.81, Dec. + 16°3, 0.25 by 0.25 mm cell + Fabry lens, 2 μ grating, 2 μ filter, slitless, (Mars image ≃ 1.5 mm) and 1.0 mm, scan 25/2, τ = 5.5 sec. *Lower* spectrum: H.A. 0^h11^m-0^h39^m W, *upper* spectrum: H.A. 0^h48^m-1^h16^m W. Dotted line represents lunar comparison profile, Figure 18. Vertical lines at λ = 2.14 and 2.18 μ are boundaries of 2 ν_3 isotopic band of CO_2 as observed on Venus. Martian absorption is confined between these boundaries, confirming identification.

Fig. 18. Moon, 1.92-2.50 μ, December 14, 1962, three scans, for comparison with Mars in Figure 17. T = 41° F, H = 0.81, Dec. + 19°8, 0.25 by 0.25 mm cell + Fabry lens, 2 μ grating, 2 μ filter, slits 1.5 and 1.0 mm, scan 5/0.5, τ = 1 sec. *Upper* spectrum: H.A. 1^h11^m-1^h17^m W, *middle* spectrum: H.A. 1^h19^m-1^h25^m W, *lower* spectrum: H.A. 1^h33^m-1^h39^m W.

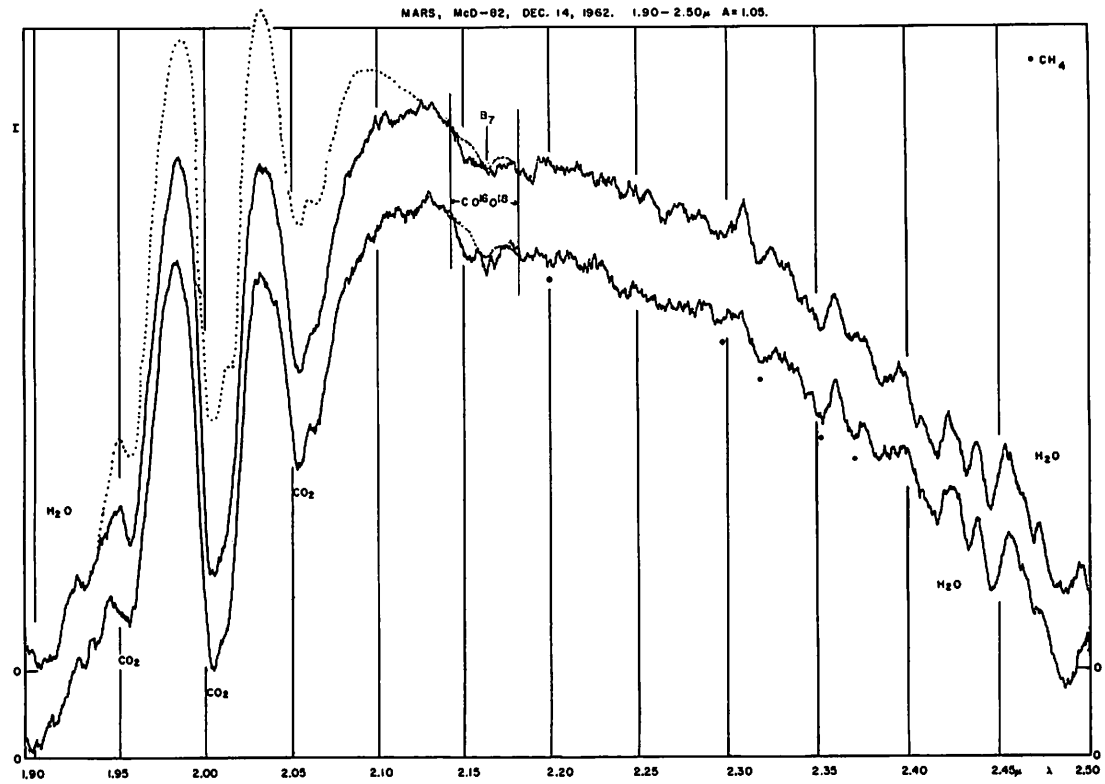
MARS, McD-82, DEC. 14, 1962. 1.90-2.50μ A=1.05.
• CH4
B7
C O16O18
H2O
CO2
CO2
CO2
H2O
H2O
I
0
0
1.90
1.95
2.00
2.05
2.10
2.15
2.20
2.25
2.30
2.35
2.40
2.45μ
λ
2.50

17.

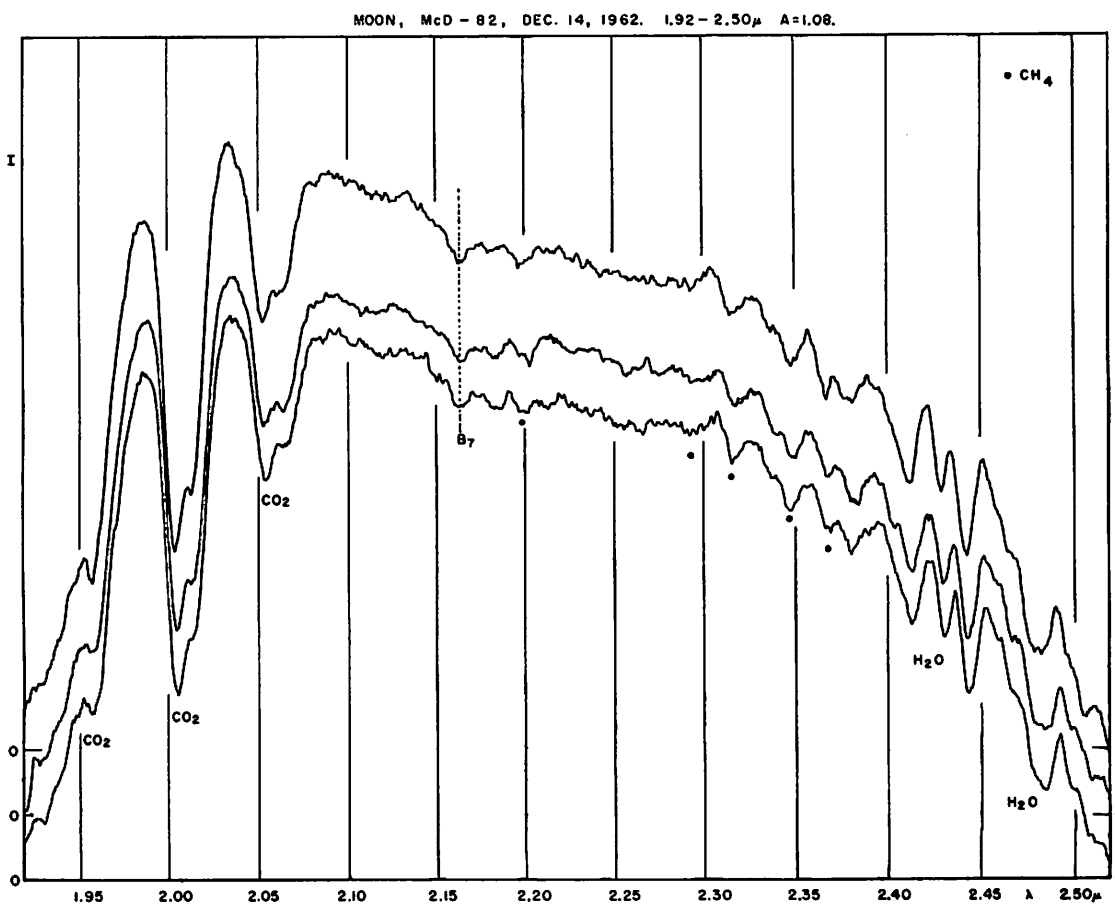
MOON, McD - 82, DEC. 14, 1962. 1.92 - 2.50μ A=1.08.
• CH4
I
B7
CO2
CO2
CO2
H2O
H2O
0
0
0
0
0
0
1.95
2.00
2.05
2.10
2.15
2.20
2.25
2.30
2.35
2.40
2.45
λ
2.50μ

18.

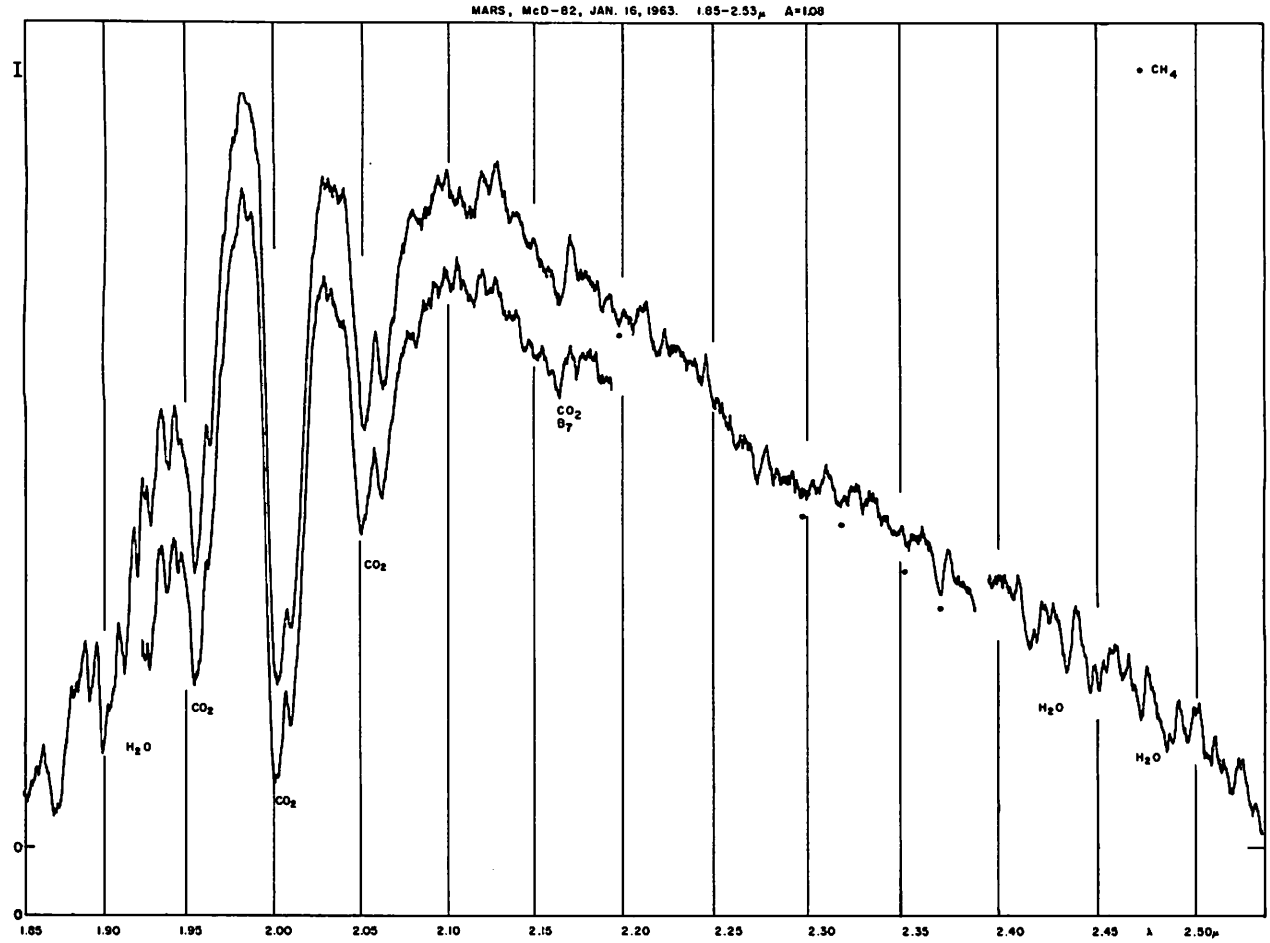

Fig. 19. Mars, 1.85-2.53 μ, January 16, 1963, two scans. T = 33° F, H = 0.52, Dec. + 18°2, cell 0.1 mm, 1.6 μ grating (increased resolution), 2 μ filter, slitless and 1.0 mm slit, scan 25/5, τ = 20 sec. *Lower* spectrum: H.A. 2^h12^m-2^h49^m, *upper* spectrum: H.A. 0^h38^m-2^h08^m W.

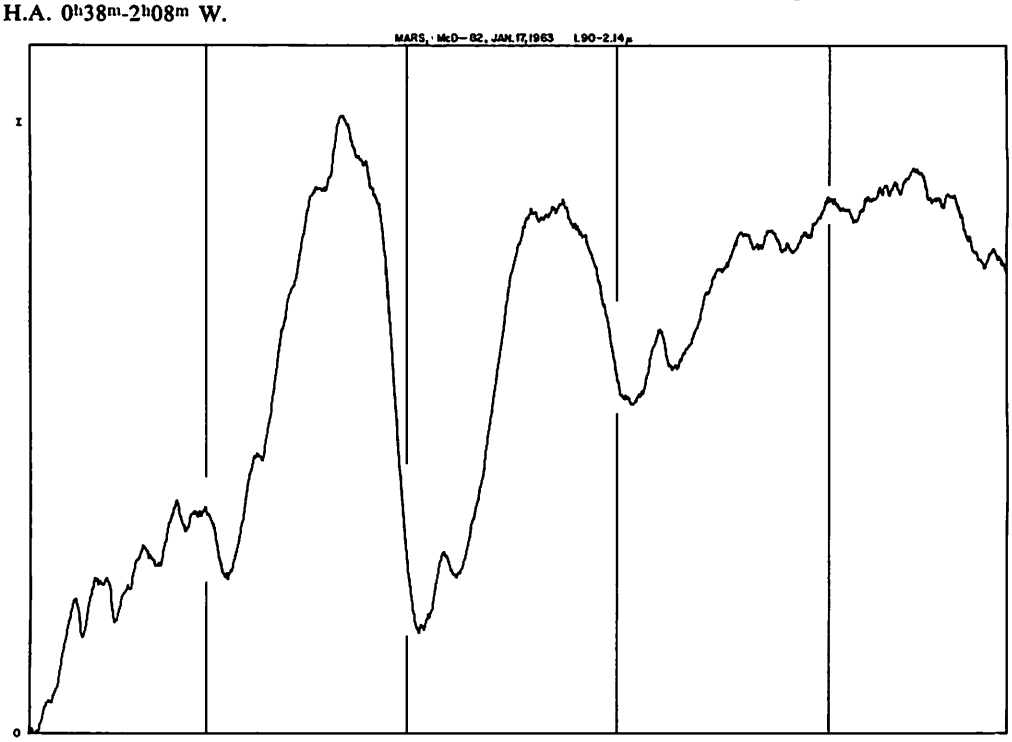

Fig. 20. Mars, 1.90-2.14 μ, January 17, 1963, Dec. + 18°3, H.A. 2^h36^m-3^h02^m W, cell 0.1 mm, 1.6 μ grating (increased resolution), 2 μ filter, slitless and 1.0 mm, scan 25/2, τ = 20 sec.

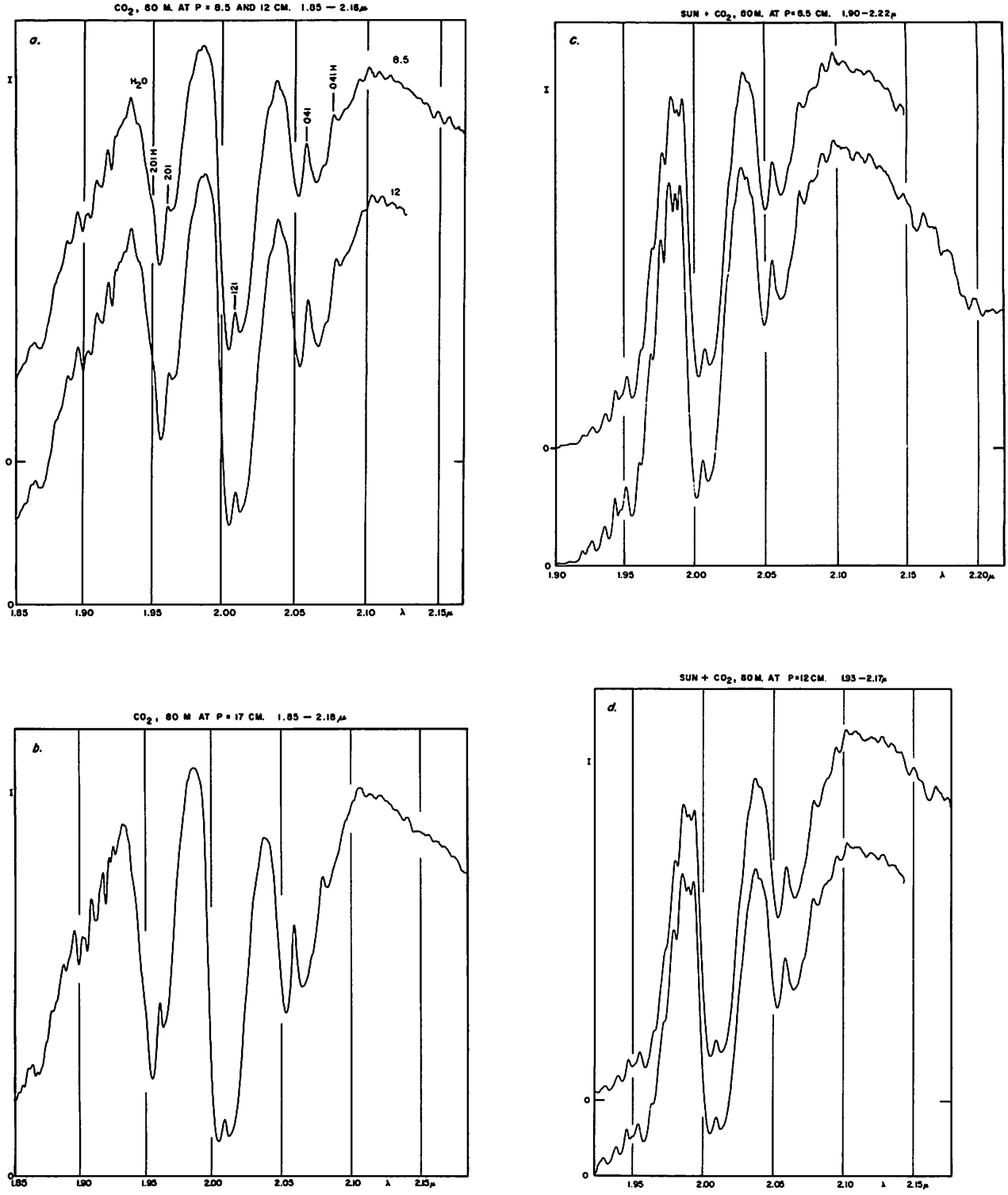

Fig. 21. a, b: Laboratory spectra of CO_2, 1.85-2.17 μ, 80 meters at p = 8.5, 12, and 17 cm: *c, d*: solar spectra, 1.90-2.20 μ, observed through 80 meters of CO_2 at p = 8.5 and 12 cm; June 13 and 14, 1963; all with 0.25 mm cell, 2 μ grating, 2 μ filter, 0.3 mm slit, scan 12.5/1.

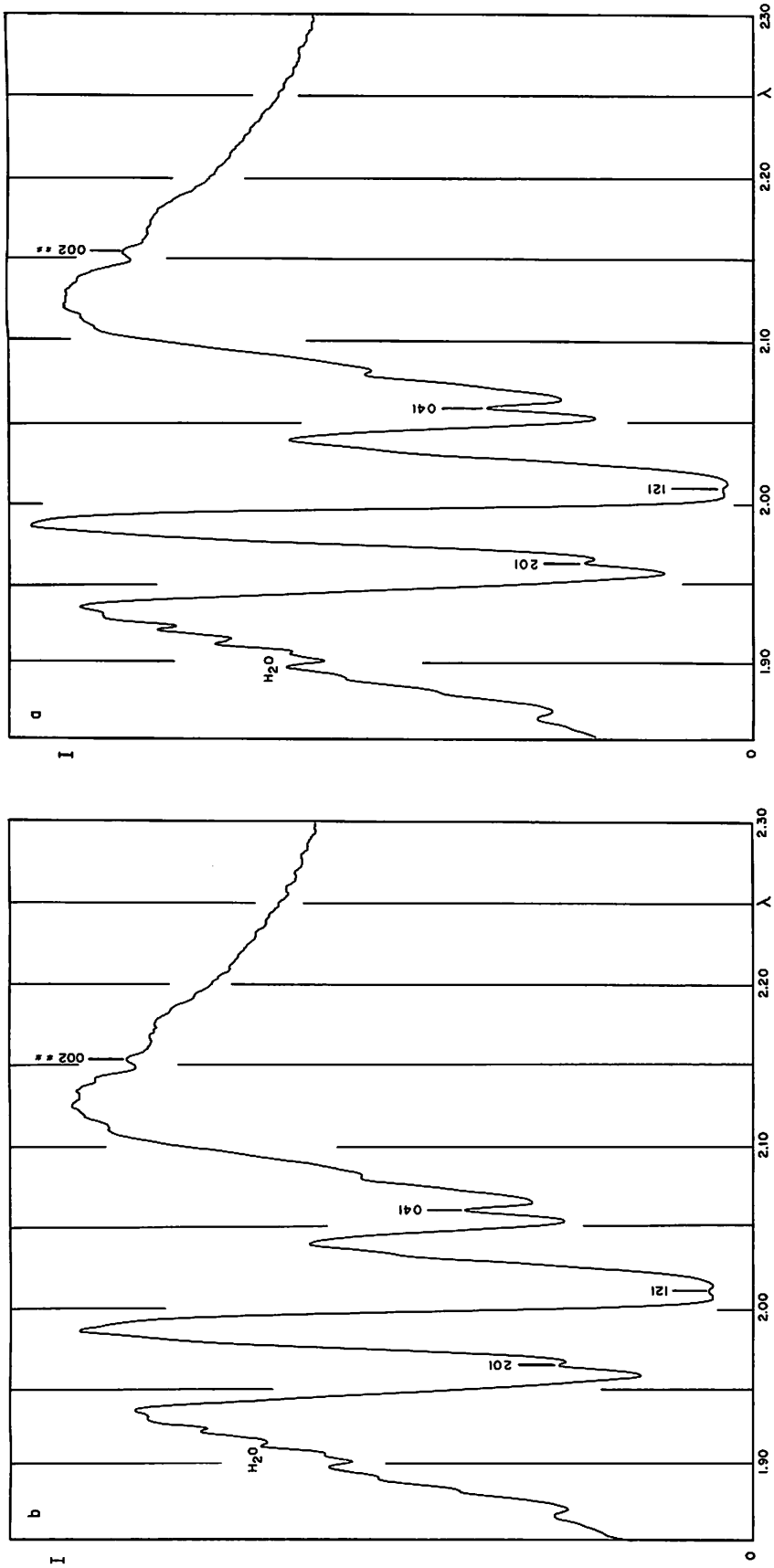

Fig. 22. Laboratory spectra of CO_2, 1.85-2.30μ. (a) 360 meters at $p = 12$ cm. (b) 1440 meters at $p = 6$ cm. Cf. measures in Table 5.

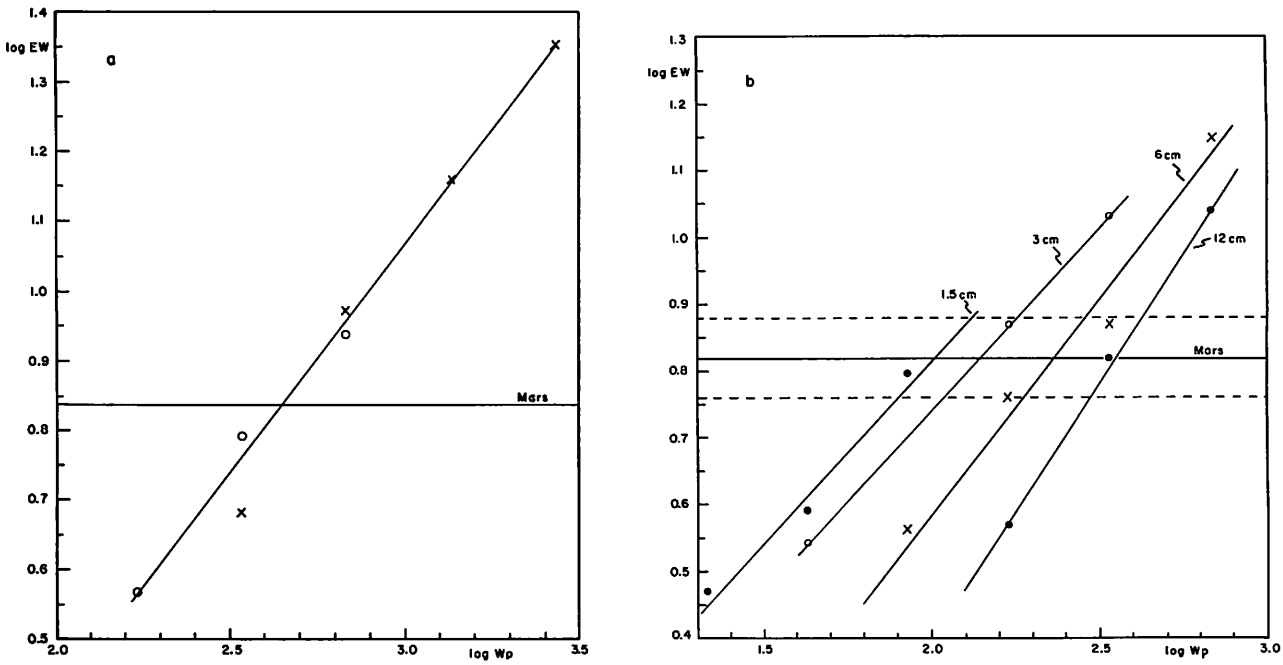

Fig. 23. (a) Equivalent widths (EW) in Å vs. *wp* for λ 2.15 μ of $C^{12}O^{16}O^{18}$ based on laboratory measures (Cf. Table 5) with intensity of band in Mars spectra indicated. (b) Measurements of λ = 1.5377 μ band of $C^{12}O_2{}^{16}$ for comparison with isotopic band shown in (a), with intensity of Mars band and its margin of uncertainty indicated.

the linear relation

$$\log \mathrm{EW} = 0.654 \log wp - 0.894. \qquad (5)$$

The coefficient of *wp* indicates that EW increases with a power of *wp* intermediate between 1 and ½ (in accordance with the fact that the band is rather weak). If this relationship holds down to the low mean pressure of the Martian atmosphere (with the rotational lines getting narrower but deeper, keeping EW constant) then one finds from EW = 7Å the value of log *wp* = 2.65. In part because the pressure broadening of the Martian CO_2 bands is caused mostly by gases other than CO_2 (cf. *Comm.* No. 32), the appropriate value of *p* in the derivation of *w* is not readily estimated.[1] Therefore, a differential method is used, comparing the λ 2.15 μ band of $C^{12}O^{16}O^{18}$ with a band of similar strength due to $C^{12}O_2{}^{16}$, the 301 band at λ = 1.5377. This latter band has on the Mars spectra of Figure 12 a mean EW = 6.6 ± 1Å; the dotted lines shown are based on the lunar spectrum of Figure 11.

Laboratory calibrations of the 301 band were taken from the spectral runs made for *Comm.* No. 32. The results are listed in Table 6, and are plotted in Figure 23b. Clearly, the representation of EW by *wp* is not very suitable for this band. The cause for this is seen from Figure 14 of *Comm.* No. 32, which shows that the pressure dependence of EW is not $p^{1/2}$ but $p^{1/4}$, though the dependence on *w* is not far from $w^{1/2}$. As a result the values obtained at lower pressures are displaced to the left in the diagram. The intersect of the relation for the equivalent Martian pressure is therefore uncertain[1] but definitely occurs well below log *wp* = 2.65, defined in Figure 23a. This indicates that the O^{18}/O^{16} ratio in the Martian atmosphere is *larger* than in the terrestrial atmosphere. A more complete laboratory study of this problem is being undertaken and distinctly improved observations of Mars will be possible early 1965 with a 5-inch beam IR spectrometer now completed. The precise O^{18}/O^{16} ratio for Mars is, of course, of great interest for the photochemical history of the Martian atmosphere and the Martian escape rate of oxygen.

Another isotopic band, λ 1.47 μ of $C^{13}O_2{}^{16}$, is in Figures 12 and 13 too heavily contaminated with telluric H_2O to give the C^{13}/C^{12} isotopic ratio, which for Venus was indeed determinable. It should be possible to detect this band from a high-altitude station, where a Martian spectrum somewhat resembling Figure 14 should be obtainable.

Other gases whose presence was tested are

[1]The discussion in *Comm.* No. 32 would indicate that for $C^{12}O_2{}^{16}$, $w \simeq 150$, $p \simeq 0.3$, $\log pw \simeq 1.7$.

TABLE 6

EQUIVALENT WIDTHS IN Å OF λ 1.538 OF $C^{12}O_2^{16}$
(second entries are logarithms)

PATHLENGTH (METERS)	$p = 1.5$ cm		$p = 3$ cm		$p = 6$ cm		$p = 12$ cm	
90.....	....	....	....	....	....	....	3.7	0.57
180.....	....	....	....	....	3.66	0.563	6.6	0.82
360.....	....	....	3.45	0.54	5.76	0.76	11.0	1.04
720.....	2.97	0.47	5.05	0.70	7.4	0.87	....	....
1440.....	3.9	0.59	7.45	0.87	14.05	1.148	....	....
2880.....	6.27	0.797	10.8	1.033	....	....	....	....

CO, CH_4 NH_3, H_2S, NO, N_2O, $COCl_2$, HCHO, and COS. The discussion follows an earlier effort (Kuiper 1952, Table 9) but with increased resolution. The results are all negative, with the limits attained stated below. The precision can probably be improved by a further order of magnitude during the next Mars opposition with improved equipment now completed.

The CO test is best made from the (2,0) band at λ 2.35 μ. The laboratory calibration may be taken from Figure 25 of the Venus study (*Comm.* Vol. 1, p. 115). No evidence for the presence of CO was found, with 4 cm atm placed as the upper limit. This corresponds to *1 cm atm in a vertical column on the planet.*

For the other gases it was necessary to obtain new laboratory comparisons. This work was done jointly with Mr. Dale Cruikshank, graduate-student assistant in this Laboratory. Because of the interest these laboratory runs have for future work as well, a set of them is being published in *Comm.* No. 34.

Several CH_4 bands are suitable for the tests: at λ 1.6657 μ, 2.199 μ, the overlapping system between 2.25-2.30 μ, the bands at 2.3165 μ and 2.373 μ. These features have been marked with dots in Figures 12, 13, 17, and 18. A close comparison between the lunar records and those of Mars show that within the precision of the data the CH_4 features in the Mars spectra are entirely telluric, which puts an upper limit of about 0.4 cm atm for the Martian contribution or 1 mm in a vertical column on the planet. This limit is 100 times less than the earlier limit (Kuiper, 1952).

The ammonia tests yield the following results. The λ 1.515 μ band gives for Mars $\leq$ 11 cm at 10 cm pressure or 1.5 cm atm. The λ 1.98 μ band gives $<$ 0.5 cm atm, 1/3 of the above amount, also observed at $p = 10$ cm. The NH_3 bands between 2.2-2.3 μ give $<$ 0.4 cm atm at $p = 10$ cm. The amount in a vertical column is therefore $<$ 1 mm atm measured at $p = 10$ cm, an amount 20 times less than the limit derived previously (Kuiper, 1952).

For N_2O no strong bands exist for $1\mu < \lambda < 2\mu$. The band at λ 2.10 μ makes the Martian equivalent absorption $<$ (2/3) 11 cm path at $p = 3$ cm; whereas the λ 2.25 μ yields $\leq$ 11 cm at $p = 3$ cm. The former test is therefore somewhat sharper and yields 0.3 cm atm at $p = 3$ cm or 0.8 mm atm for the vertical column (measured at $p = 3$ cm), an improvement by the factor of 2500 over the earlier limit (Kuiper, 1952).

The tests for NO are not sensitive. The λ 1.79 μ band gives $<$ 60 cm at 1.26 atm. The upper limit for the vertical column is therefore approximately 20 cm atm, measured at $p = 1.26$.

The test for H_2S in the spectral region covered is not sensitive either. The λ 1.58 μ band gives $<$ 30 cm at $p = 1$ atm or $<$ 7.5 cm atm for the vertical column.

A test was made for $COCl_2$ but no prominent bands exist between 1-2.5μ for a 10 cm path at 1 atm; the test must be repeated in another spectral region.

HCHO (formaldehyde) shows a prominent band at 2.27 μ with 11 cm path at 1 atm. The Martian content of this gas is well below one-tenth of this amount or $<$ 0.3 cm atm in the vertical column.

COS (carbonyl sulphide) was examined on a 5 cm path at $p = 1$ atm. A very strong band occurs at 2.44 μ. The Martian atmospheric content must be $<<$ 0.2 cm atm in a vertical column.

The problem of NO_2 (nitrogen dioxide), a widely debated topic, is examined by Mr. Marshall in *Comm.* No. 35. Because many electronic bands can be observed in the accessible photographic region the best test for the presence of this gas on Mars is not in the infrared but in the photographic spectrum.

7. *Ratio Spectra, Mars : Moon*

The Martian and lunar records here reproduced allow the derivation of approximate *ratio spectra* in which the spectral distribution of Mars is expressed

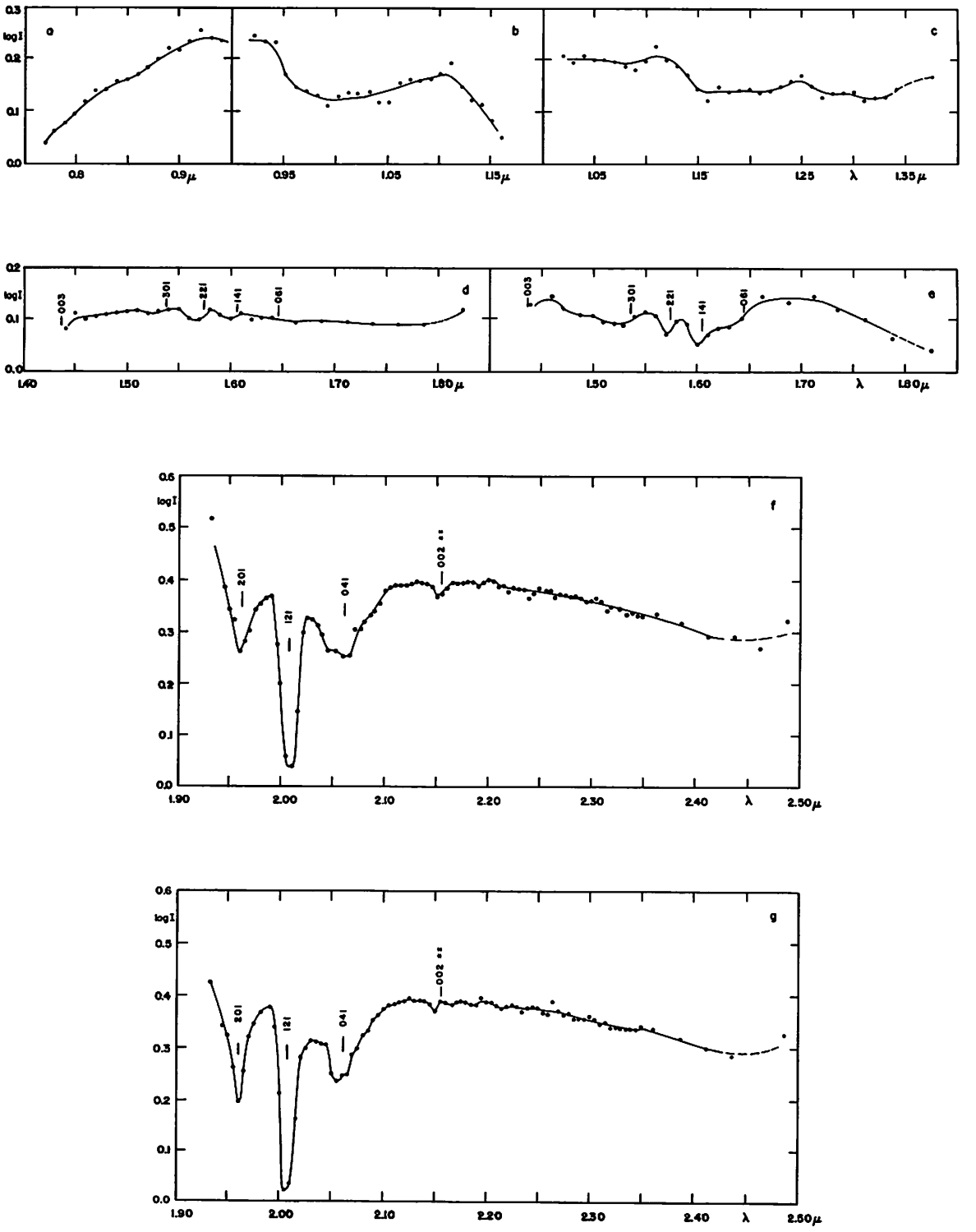

Fig. 24. Spectral intensity ratios Mars/Moon, on logarithmic scale (a) 0.75-0.96 μ, from Figs. 4 and 5; (b) 0.92-1.17 μ, Figs. 6 and 7; (c) 1.02-1.4 μ, Figs. 8 and 9; (d) 1.43-1.85 μ, Figs. 10 and 11; (e) 1.43-1.85 μ, Figs. 12 and 11; (f) 1.92-2.5 μ, Figs. 17 and 18 (measured by GPK); (g) 1.92-2.5 μ, Figs. 17 and 18 (measured by SML).

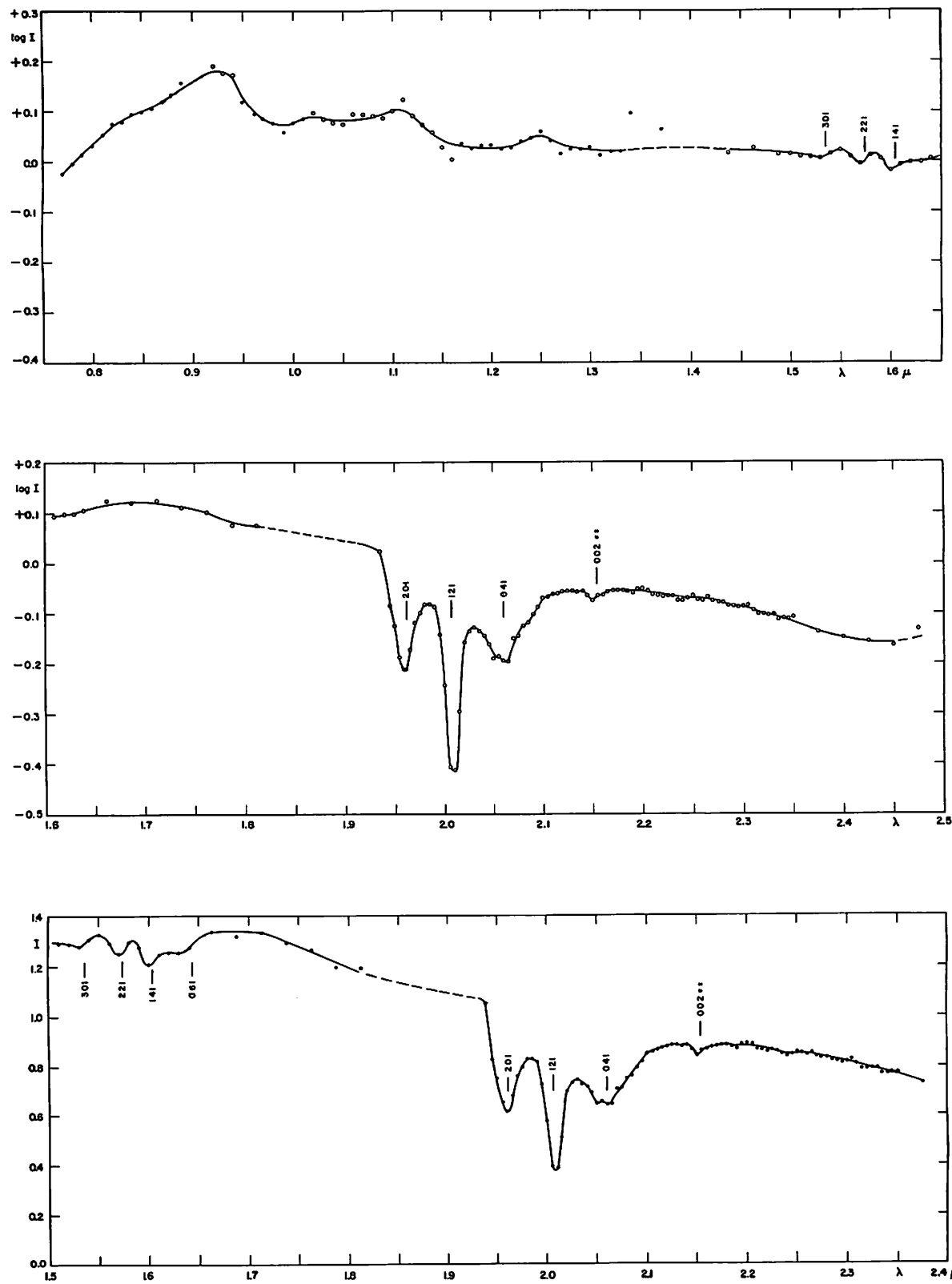

Fig. 25. Spectral intensity ratios Mars/Moon, consolidated. *Upper* and *middle:* average of ratios plotted in Fig. 24 logarithmically combined by vertical adjustments of overlapping sections; *lower:* 1.5-2.5 μ as above but replotted on intensity scale. Martian CO_2 bands identified. Filled circles are single measures, open circles averages in overlapping areas.

in terms of the lunar continuum. Both the telluric and the solar absorptions are thus in principle eliminated though the data will be poor within the heavy H_2O telluric absorptions owing to low residual intensities. The ratios here derived suffer further from one weakness that in principle can be remedied; namely, that the lunar image slowly drifted over the spectrometer slit since no declination drive was used on the telescope. As has been stated, the effects of this drift were minimized by using a grossly-extrafocal lunar image and by making the lunar scans at a rapid rate. Further, several lunar scans were used when practicable.

The ratio measures were made at preselected closely-packed wavelength intervals, using the original spectral traces after a somewhat smoothed interpolation curve had been drawn on them to minimize the random effects of electronic noise. The measures were made by a student-assistant, Mr. S. M. Larson, except for the second set of measures of the 1.9-2.5 μ region which was made by the writer. In this second set, separately reproduced in Figure 24, special attention was paid to the maxima and the minima of the Mars and Moon records, for possibly-improved wavelength consistency.

The heavy telluric H_2O absorptions near 1.4 μ and 1.9 μ cause two breaks in the ratio spectra, indicated by dashes in Figure 25. The relative ordinates of the three segments were placed in approximate accordance with low-disperson runs covering the entire region 0.5-2.5 μ. The positioning of the segments between 0.75-1.4 μ was made from the short overlapping portions.

The ratio spectra so found are shown in Figures 24 and 25. They are considered provisional, particularly with respect to the secondary features between 0.8-1.2 μ, some of which may be due to inadequate lunar calibration. The 1.6 μ region should be fairly precise but the CO_2 bands near 2.0 μ require interpretation, as follows from the discussion accompanying Figure 16b. The measurement of the Martian CO_2 bands can be made unambiguously only during such periods as have either a complete separation of the telluric and Martian rotational lines (as occurred for the 1.6 μ bands; see Figure 16a), or else a central superposition (when Mars is at opposition and has zero radial velocity). During the next opposition the techniques employed here will be further developed.

Acknowledgments. I am indebted to Dr. W. W. Morgan and his staff for making the 82-inch telescope available for the Mars observations; to Dr. H. Johnson for his frequent advice on technical problems; to Mr. A. Binder and Mr. D. Cruikshank for assistance in the observations; to Dr. B. M. Herman of the Institute of Atmospheric Physics for making the computations reproduced in Tables 1-3 and Figures 1-3; to Dr. J. E. McDonald for his advice in the preparation of Section 3; to Mr. T. Owen for his indispensable assistance in the laboratory CO_2 calibrations; to Mr. D. Cruikshank for his assistance with the calibrations described in Sec. 6; to Mrs. Linda Scheer and Miss T. R. McKinney for assistance with the diagrams; and to Mr. S. M. Larson for his assistance in the computations of Tables 1-3 from the machine data, his assistance in Sec. 7, and in the production of Figures 24 and 25.

The program of infrared planetary spectroscopy is supported by the National Aeronautics and Space Administration through Grant No. NsG 161-61.

Note added in proof. The comment on p. 81 regarding the distribution of Martian haze is independent of the occasional presence, repeatedly reported, of what appears to be a surface frost deposit near the sunrise terminator. Such a surface deposit would clearly depend on the daily temperature of the planetary surface.

It has been pointed out to me by Dr. Frank A. Gifford that the Martian dust storms discussed on pp. 89 and 90 could involve saltation of dust particles. I am assuming, however, that the widespread haze condition of the Martian atmosphere usually following local dust storms indicates the presence of airborne dust, as discussed above.

REFERENCES

Antoniadi, E. M. 1930, *La Planète Mars* (Paris: Hermann), pp. 45-46.

Coblentz, W. W. 1926, *Pop. Astron., 33,* 370.

Dallavalle, J. M. 1948, *Micromeritics* (2nd ed.; New York, Toronto, and London: Pitman Pub. Corp.).

de Vaucouleurs, G. 1954, *Physics of the Planet Mars* (London: Faber and Faber).

Dollfus, A. 1961, *Planets and Satellites,* ed. G. P. Kuiper and B. M. Middlehurst (Chicago: University of Chicago Press), Chap. 9.

——— 1963, presentation at NASA Meeting, Washington, D.C., October 1, 1963.

——— 1964, *l'Astronomie, 78,* 41-56.

Finsen, W. S. 1961, *Planets and Satellites,* ed. G. P. Kuiper and B. M. Middlehurst (Chicago: University of Chicago Press), Chap. 17.

Fletcher, N. H. 1962, *The Physics of Rainclouds* (Cambridge: Cambridge University Press).

Fuks, N. A. 1955, *The Mechanics of Aerosols,* trans. E. Lachowicz (Washington: U.S. Department of Commerce).

Gehrels, T. and Teska, T. M. 1962, *Comm. LPL, 1,* 173.

Grandjean, J. and Goody, R. M. 1955, *Ap. J., 121,* 548.

Green, H. L. and Lane, W. R. 1957, *Particulate Clouds: Dusts, Smokes, and Mists* (Toronto, London, and New York: D. Van Nostrand).

Greenfield, S. M. 1956, *J. Meteor., 14,* 115-125.

Harris, D. L. 1961, *Planets and Satellites,* ed. G. P. Kuiper and B. M. Middlehurst (Chicago: University of Chicago Press), Chap. 8.

Humason, M. L. 1961, *Ibid.,* Chap. 16.

Junge, C. E. 1963, *Air Chemistry and Radioactivity* (New York and London: Academic Press).

Kaiser, F. 1872, *Ann. Leiden Obs., 3.*

Kuiper, G. P. 1931, *Hemel en Dampkring, 29,* 224, 228-229.

——— 1947, Harvard College Observatory Announcement Card 851.

——— 1949, *The Atmospheres of the Earth and Planets,* ed. G. P. Kuiper (1st ed.; Chicago: University of Chicago Press), Chap. 12.

——— 1952, *Ibid.,* (2nd ed.), Chap. 12.

——— 1963, *Mémoires Soc. R. Sc. Liège,* Series 5, Vol. 9.

Liais, E. and Cruls, L. 1878, *Mémoire de Mars* (Rio de Janeiro).

McDonald, J. E. 1964, *J. Atmos. Sci., 21,* 13 ff. and in press.

Mohler, O. C., Pierce, A. K., McMath, R. R., and Goldberg, L. 1950, *Photometric Atlas of the Near Infra-red Solar Spectrum, λ 8465 to λ 25,242* (Ann Arbor: University of Michigan Press.)

Schatzman, E. 1951, *Comptes Rendus* (Paris), *232,* 692.

Sinton, W. M. 1961, *Planets and Satellites,* ed. G. P. Kuiper and B. M. Middlehurst (Chicago: University of Chicago Press), Chap. 11.

Slipher, E. C. 1962, *Mars 1905-1961,* Chap. 5.

Spinrad, H., Münch, G., and Kaplan, L. D. 1963, *Ap. J., 137,* 1319-1321.

——— 1964, *Ibid., 139,* 1.

Trouvelot, E. L. 1884, *Comptes Rendus* (Paris), *98,* 789.

Van de Hulst, H. C. 1952, *The Atmospheres of the Earth and Planets,* ed. G. P. Kuiper (2nd ed.; Chicago: University of Chicago Press), Chap. 3.

Weaver, H. F. *et al.* 1963, presentation at AAS Meeting, Tucson, Arizona, April 1963.